Early neurulation recapitulated in assemblies of embryonic and extraembryonic cells

Noémie M. L. P. Bérenger-Currias[1,2], Maria Mircea*[1], Esmée Adegeest*[1], Patrick R. van den Berg[1], Marleen Feliksik[1], Mazène Hochane[#,1], Timon Idema[#,2], Sander J. Tans[#,2,3], Stefan Semrau[#,1]

* equal contribution
# co-corresponding authors
1. Leiden University, Einsteinweg 55, 2333 CC Leiden, Netherlands
2. Delft University of Technology, Department of Bionanoscience, Kavli Institute of Nanoscience, Van der Maasweg 9, 2629 HZ Delft, Netherlands
3. AMOLF, Science Park 104, 1098 XG Amsterdam, Netherlands

Recapitulating mammalian embryonic development *in vitro* is a major challenge in biology. It has been shown that gastruloids[1-5] and ETX embryos[6] can display hallmarks of gastrulation *in vitro*. However, these models fail to progress beyond spatially segregated, yet amorphous cellular assemblies. Systems such as organoids[7] do show tissue stratification and organogenesis, but require adult stem cells or exogeneous induction of specific cell fates, and hence do not reflect the emergent organization of embryonic development. Notably, gastruloids are derived exclusively from embryonic stem cells (ESCs), whereas, *in vivo*, crucial patterning cues are provided by extraembryonic cells[8]. Here, we show that assemblies of mouse ESCs (mESCs) and extraembryonic endoderm (XEN) cells can develop beyond gastrulation and produce a central hallmark of organogenesis: stratified neural epithelia resembling a neural tube, which can be further differentiated to cerebral cortex-like tissue. By single-cell RNA-seq, we show that our

model has a larger cell type diversity than existing models, and that mESCs and XEN cells impact each other's differentiation. XEN cells promote neural tube formation through local inhibition of primitive streak formation. In turn, the presence of mESCs drives XEN cells to resemble visceral endoderm, which envelops the embryo *in vivo*. This study provides a model system to investigate neurulation and extraembryonic endoderm development, and may serve as a starting point to generate embryo models that advance further toward the formation of the vasculature, nervous system, and digestive tube.

We first implemented the original mouse gastruloid protocol[1] in which mESCs are aggregated in N2B27 media and exposed to a pulse of WNT signaling for 24 h. After 96 h, this protocol resulted in elongated gastruloids. As reported before[1-3], gastruloids contained localized primitive streak- and neural progenitor-like compartments, marked by Brachyury (T) and SOX2, respectively (Fig. 1b, inset). We then adapted the gastruloid protocol by co-aggregating XEN cells with mESCs, keeping all other conditions the same (Fig. 1a). After 96 h, the resulting aggregates again showed T-positive and SOX2 positive compartments (Fig. 1b). However, in striking contrast with standard gastruloids, SOX2-positive cells were now organized in stratified epithelia surrounding one or multiple lumina. The frequency of these tubular structures depended on the fraction of XEN cells (Fig. 1c, Extended Data Fig. 1a). At a XEN:mESC ratio of 1:3 we observed the concurrence of SOX2-positive tubes and T-positive cells in the majority of aggregates. Since the canonical pluripotency marker OCT4 was not expressed (Extended Data Fig. 1b), we hypothesized that the observed structures resemble neural tubes. The presence of N-cadherin and absence of E-cadherin in the tubes (Fig. 1d) is consistent with the known switch from E- to N-cadherin during neural differentiation *in vivo*[9] and *in vitro*[10]. Furthermore, we detected the neural progenitor markers PAX6 and NKX6.1[11] in subpopulations of the SOX2-positive cells (Fig. 1e). Taken together, our results suggested that

mESC-XEN aggregates can recapitulate elements of neural induction without relying on externally applied signals, thereby mimicking embryonic development. Hence, we consider this model system to be a 'neuruloid'.

Next, we wanted to exclude that all mESCs are biased towards the neural fate, as occurs in existing protocols for induction of neural epithelia[12-14]. To quantify cell type diversity, we characterized neuruloids and regular gastruloids (without XEN cells), as well as undifferentiated mESCs and XEN cells, with single-cell RNA-sequencing (scRNA-seq) (Extended Data Fig. 2a-e). By mapping the data to single-cell transcriptomes of mouse embryos from E6.5 to E8.5[15] (Extended Data Fig. 2f-i) we classified the transcriptional identity of the cells (Fig. 2a-c). Except for the least abundant cell types, the distribution of cell types was consistent across two biological replicates (Extended Data Fig. 2h). Expression of known markers confirmed the classification by mapping to *in vivo* data (Extended Data Fig. 3, Supplementary Table 1). Most cell types belonged to the E8.0 or E8.5 embryo (Fig. 2d), which indicates that *in vitro* differentiation proceeded roughly with the same speed as *in vivo* development. Most importantly, the cell type distribution in neuruloids was at least as diverse as in gastruloids. Both model systems contained a variety of mesodermal cell types, such as paraxial or somitic mesoderm, as well as anterior cell types, such as spinal cord- or brain-like cells (Fig. 2c). Neuromesodermal progenitors (NMPs) and spinal cord-like cells were the most abundant in both systems. Neuruloids also contained cell types that were not detected in gastruloids, such as extraembryonic endoderm cell types, as well as nascent or pharyngeal mesoderm. Extraembryonic endoderm exclusively differentiated from XEN cells, as evident from experiments using GFP-expressing XEN cells in neuruloids (Fig. 2e). In summary, neuruloids have increased cell type diversity compared to gastruloids.

At the resolution achieved by mapping to the *in vivo* dataset, gastruloids and neuruloids contained the same neuroectodermal cell types. That did not rule out the possibility of gene expression differences between neuroectoderm in the two model systems. We used the neural tube markers *Sox2*, *Pax6* and *Nkx6.1*[11], detected in the tubular structures (Fig. 1e), to identify the corresponding cells in the scRNA-seq data. We found these markers to be co-expressed in cells classified as "spinal cord" in the scRNA-seq data (Fig. 2f, Extended Data Fig. 4a). A large number of canonical neural tube markers is differentially expressed in those cells (Fig. 2g, Extended Data Table 1), which further supports their characterization as neural tube-like. Mapping of the spinal cord-like cluster in neuruloids to *in vivo* spinal cord (Extended Data Fig. 4b) showed that the cells were most similar to dorsal neural progenitors *in vivo*. Differential gene expression analysis between the spinal cord-like cluster in gastruloids and neuruloids (Fig. 2h) revealed a higher expression of dorsal markers in neuruloids. Several of these markers, such as PAX3, MSX1 or ZIC1 are known to be induced by BMP signaling (Extended Data Table 2), which might be activated by BMP2 originating in XEN-derived cells (Extended Data Fig. 4c). In summary, tubular structures in neuruloids are composed of cells that have a neural progenitor-like transcriptional profile. Compared to gastruloids, neuruloids push the neural progenitors towards a dorsal identity.

We performed experiments to investigate how strongly the neural tube-like structures resemble their *in vivo* counterparts. Time-lapse imaging of the neural progenitor marker SOX1 in developing neuruloids revealed an amorphous SOX1 positive population prior to the formation of SOX1 positive tubes (Fig. 3a, Supplementary videos 1-3). In gastruloids, by contrast, SOX1 remained restricted to an amorphous subpopulation (Fig. 3a, Supplementary videos 4-6). The sequence observed in neuruloids mimics *in vivo* mouse development, where SOX1 is first expressed in the neural plate and persists in the neural tube[16].

To explore, how the neural tube-like structures respond to signaling inputs found *in vivo*, we studied role of the BMP, Hedgehog (Hh) and retinoic acid (RA) pathway (Fig. 3b-c). BMP signaling has been shown to prevent premature specification of neural fates[17]. Consistently, BMP inhibition resulted in a higher frequency of neural progenitors (marked by PAX6 and NKX6.1). Sonic hedgehog, which originates on the ventral side of the developing neural tube *in vivo*, elicits ventral characteristics in the neural progenitors[18]. As expected, activating the Hh pathway in our experiments resulted in more cells with ventral characteristics (indicated by the presence of NKX6.1). RA is involved in anterior-posterior patterning and neurogenesis[19]. In our *in vitro* model, adding RA strongly increased the number of cells expressing PAX6, which is found specifically in anterior progenitors[20]. In summary, signaling experiments showed that neural tube-like structures in neuruloids respond to signaling cues as expected from *in vivo* development.

The similarity with neural tubes *in vivo* suggested that the tubular structures might be able to further differentiate to cerebral tissue. Indeed, when neuruloids were cultured for an additional 4 days in appropriate differentiation media[21], layered cerebral cortex-like tissues surrounding cavities, reminiscent of ventricles, could be observed (Fig. 3d, Extended Data Fig. 5a). Intriguingly, we also observed small clusters of cells positive for the endothelial marker CD31 (Extended Data Fig. 5b), which might indicate early stages of a developing vasculature. Taken together, immunostaining, time-lapse imaging, signaling and differentiation experiments revealed properties of neural tubes developing *in vivo*.

Having characterized the neural tube-like structures, we next focused on the XEN cells, their differentiation in the neuruloids and their role in inducing the tubes. Strikingly, XEN cells

always formed the outermost layer of the neuruloids (Fig. 1b, Extended Data Fig. 1a), resembling *in vivo* extraembryonic endoderm, which envelops the embryo. Consistently, the transcriptional profiles of XEN-derived cells in neuruloids mapped to extraembryonic endoderm (parietal endoderm (PE), and visceral endoderm (VE)) in the *in vivo* data set[15]. Interestingly, some XEN-derived cells also mapped to gut, reminiscent of the contribution of VE to the gut *in vivo*[22,23] (Fig. 4a, Extended Data Fig. 6a). By contrast, undifferentiated XEN cells exclusively mapped to PE, as reported previously[24,25]. Mapping to an (extraembryonic-) endoderm-focused dataset[23] gave a similar result (Extended Data Fig. 6b-c). Differential gene expression analysis revealed several PE and VE markers to be more highly expressed in undifferentiated XEN or differentiated XEN in neuruloids, respectively (Fig. 4b, Extended Data Table 3). These results suggested that XEN cells differentiate from a PE- to a VE-like state in neuruloids.

Since PE and VE have fairly similar gene expression patterns, we wanted to confirm the differentiation of XEN cells with a more sensitive method. We carried out single-molecule FISH on the PE marker *Fst*[26], the VE marker *Spink1*[27] and the pan-extraembryonic endoderm marker *Dab2*[28] (Fig. 4c). Whereas XEN cells in neuruloids only showed *Dab2* and the VE marker, undifferentiated XEN cells broadly co-expressed all markers, even when they were exposed to WNT signaling in the same way as neuruloids. Subpopulations of XEN cells in neuruloids also expressed E-cadherin, a VE marker[29] (Fig. 4d), whereas the anterior VE marker *Hhex*[30] was not detected by single-molecule FISH (Extended Data Fig. 6d). These results suggest that undifferentiated XEN cells have both PE and VE characteristics but become more VE-like due to the presence of mESCs. Neuruloids thus mimic *in vivo* organization, where VE is in direct contact with the embryo and PE contributes to the yolk sac.

Next, we were wondering how XEN cells exert their effect on the co-differentiating mESCs. Focusing on neuruloids that were only partially covered with XEN cells, we observed that tubular structures were always adjacent to the XEN cells, while the primitive streak-like population (T-positive) was on the opposite side (Extended Data Fig. 1a). Notably, we could observe local suppression of the primitive streak population already prior to tube formation, at 72 h, a time point when gastruloids were still mostly spherically symmetric (Fig. 4e). This observation suggested that XEN cells guide symmetry breaking by a local effect on adjacent mESC-derived cells. This effect is reminiscent of the anterior VE *in vivo*, which breaks anterior-posterior symmetry by local inhibition of WNT signaling.

In vivo, epithelial polarity and stratification depend on the formation of a basement membrane. We therefore hypothesized that the XEN cells affect the mESCs by forming such a membrane. XEN cells indeed express the extracellular matrix components laminin and fibronectin in neuruloids (Extended Data Fig. 7a) and laminin immunostaining showed high signal between the XEN cells and the tubular structures (Fig. 4f). It has been shown previously, for small aggregates of mESCs, that the presence of an extracellular matrix can be sufficient for polarization and lumen formation[12,13,31]. Growing gastruloids in an extracellular matrix gel (Geltrex) did result in cavities, though no stratified tissues were observed (Extended Data Fig. 7b).

Since culture in Geltrex was not sufficient to yield neural tube-like structures, we next wanted to test whether diffusible factors could be responsible. Growing gastruloids in media conditioned by undifferentiated XEN cells inhibited gastruloid elongation and restricted the primitive streak-like population to the center of the gastruloids (Fig. 4g). Diffusible factors are thus likely involved in the effect of the XEN cells. One important class of factors produced by

the anterior VE *in vivo* are WNT inhibitors[32]. Since XEN cells were able to induce neural tube-like structures in the absence of exogenous WNT signal (Extended Data Fig. 7c), they might either suppress low endogenous WNT activity, or pathways other than WNT also play a role. All combined, our experiments suggest that XEN cells become VE-like in neuruloids and guide symmetry-breaking by local inhibition of primitive streak formation. Diffusible factors and the presence of a basement membrane both appear necessary for the formation of neural tube-like structures.

In this study we provide a key next step for *in vitro* models of embryonic development: we show that assemblies of mESCs and XEN cells can progress beyond gastrulation and robustly produce neural tube-like structures. Our self-organized neuruloids enable direct *in vitro* study of mammalian neurulation, and could reveal new mechanisms in extraembryonic endoderm development. Our observation that XEN cells in neuruloids differentiate due to the presence of mESCs suggests that the developing epiblast contributes to VE specification *in vivo*. Due to their high cell type diversity, neuruloids could be the basis for creating more complex models comprising tissues from several germ layers. The CD31 positive endothelial cells observed next to cerebral cortex-like tissue might be able to form a vascular network with additional signaling cues[33]. On a fundamental level, our findings indicate that reciprocal interaction between co-differentiating cell types can have critical developmental consequences. Adding XEN, or similar cell types, to existing organoid systems might trigger similar morphogenetic events as observed here. This might be particularly relevant for organoids that are currently grown in extracellular matrix gel: in our experiments, XEN cells had a bigger impact on morphogenesis than extracellular matrix alone. In conclusion, this study established a new in *vitro* model that recapitulates elements of *in vivo* neurulation and demonstrates the morphogenetic potential of heterotypic cell-cell interactions.

1. van den Brink, S. C. *et al.* Symmetry breaking, germ layer specification and axial organisation in aggregates of mouse embryonic stem cells. *Development* **141,** 4231–4242 (2014).

2. Turner, D. A. *et al.* Anteroposterior polarity and elongation in the absence of extra-embryonic tissues and of spatially localised signalling in gastruloids: mammalian embryonic organoids. *Development* **144,** 3894–3906 (2017).

3. Beccari, L. *et al.* Multi-axial self-organization properties of mouse embryonic stem cells into gastruloids. *Nature* 1 (2018). doi:10.1038/s41586-018-0578-0

4. Warmflash, A., Sorre, B., Etoc, F., Siggia, E. D. & Brivanlou, A. H. A method to recapitulate early embryonic spatial patterning in human embryonic stem cells. *Nature Methods* **11,** 847–854 (2014).

5. Simunovic, M. *et al.* A 3D model of a human epiblast reveals BMP4-driven symmetry breaking. *Nature Cell Biology* **21,** 900–910 (2019).

6. Sozen, B. *et al.* Self-assembly of embryonic and two extra-embryonic stem cell types into gastrulating embryo-like structures. *Nature Cell Biology* **20,** 979–989 (2018).

7. Takebe, T. & Wells, J. M. Organoids by design. *Science* **364,** 956–959 (2019).

8. Tam, P. P. L. & Loebel, D. A. F. Gene function in mouse embryogenesis: get set for gastrulation. *Nature Reviews Genetics* **8,** 368–381 (2007).

9. Hatta, K. & Takeichi, M. Expression of N-cadherin adhesion molecules associated with early morphogenetic events in chick development. *Nature* **320,** 447–449 (1986).

10. Punovuori, K. *et al.* N-cadherin stabilises neural identity by dampening anti-neural signals. *Development* **146,** dev183269 (2019).

11. Jessell, T. M. Neuronal specification in the spinal cord: inductive signals and transcriptional codes. *Nature Reviews Genetics* **1,** 20–29 (2000).

12. Ranga, A. *et al.* Neural tube morphogenesis in synthetic 3D microenvironments. *Proc. Natl. Acad. Sci. U.S.A.* **113,** E6831–E6839 (2016).

13. Meinhardt, A. *et al.* 3D Reconstitution of the Patterned Neural Tube from Embryonic Stem Cells. *Stem Cell Reports* **3,** 987–999 (2014).

14. Haremaki, T. *et al.* Self-organizing neuruloids model developmental aspects of Huntington's disease in the ectodermal compartment. *Nature Biotechnology* **37,** 1198–1208 (2019).

15. Pijuan-Sala, B. *et al.* A single-cell molecular map of mouse gastrulation and early organogenesis. *Nature* **566,** 490–495 (2019).

16. Pevny, L. H., Sockanathan, S., Placzek, M. & Lovell-Badge, R. A role for SOX1 in neural determination. *Development* **125,** 1967–1978 (1998).

17. Di-Gregorio, A. *et al.* BMP signalling inhibits premature neural differentiation in the mouse embryo. *Development* **134,** 3359–3369 (2007).

18. Dessaud, E., McMahon, A. P. & Briscoe, J. Pattern formation in the vertebrate neural tube: a sonic hedgehog morphogen-regulated transcriptional network. *Development* **135,** 2489–2503 (2008).

19. Maden, M. Retinoid signalling in the development of the central nervous system. *Nat. Rev. Neurosci.* **3,** 843–853 (2002).

20. Ericson, J. *et al.* Pax6 controls progenitor cell identity and neuronal fate in response to graded Shh signaling. *Cell* **90,** 169–180 (1997).

21. Lancaster, M. A. *et al.* Cerebral organoids model human brain development and microcephaly. *Nature* **501,** 373–379 (2013).

22. Kwon, G. S., Viotti, M. & Hadjantonakis, A.-K. The endoderm of the mouse embryo arises by dynamic widespread intercalation of embryonic and extraembryonic lineages. *Developmental Cell* **15,** 509–520 (2008).

23. Nowotschin, S. *et al.* The emergent landscape of the mouse gut endoderm at single-cell resolution. *Nature* **569,** 361–367 (2019).

24. Brown, K. *et al.* A comparative analysis of extra-embryonic endoderm cell lines. *PLoS ONE* **5,** e12016 (2010).

25. Kunath, T. *et al.* Imprinted X-inactivation in extra-embryonic endoderm cell lines from mouse blastocysts. *Development* **132,** 1649–1661 (2005).

26. Feijen, A., Goumans, M. J. & van den Eijnden-van Raaij, A. J. Expression of activin subunits, activin receptors and follistatin in postimplantation mouse embryos suggests specific developmental functions for different activins. *Development* **120,** 3621–3637 (1994).

27. Hou, J. *et al.* A systematic screen for genes expressed in definitive endoderm by Serial Analysis of Gene Expression (SAGE). *BMC Developmental Biology* **7,** 92–13 (2007).

28. Yang, D.-H. *et al.* Disabled-2 Is Essential for Endodermal Cell Positioning and Structure Formation during Mouse Embryogenesis. *Developmental biology* **251,** 27–44 (2002).

29. Wang, A. *et al.* Nonmuscle myosin II isoform and domain specificity during early mouse development. *Proc. Natl. Acad. Sci. U.S.A.* **107,** 14645–14650 (2010).

30. Thomas, P. Q., Brown, A. & Beddington, R. S. Hex: a homeobox gene revealing peri-implantation asymmetry in the mouse embryo and an early transient marker of endothelial cell precursors. *Development* **125,** 85–94 (1998).

31. Bedzhov, I. & Zernicka-Goetz, M. Self-Organizing Properties of Mouse Pluripotent Cells Initiate Morphogenesis upon Implantation. *Cell* **156,** 1032–1044 (2014).

32. Kimura-Yoshida, C. *et al.* Canonical Wnt signaling and its antagonist regulate anterior-posterior axis polarization by guiding cell migration in mouse visceral endoderm. *Developmental Cell* **9,** 639–650 (2005).

33. Rossi, L. F., Harris, K. D. & Carandini, M. Excitatory and inhibitory intracortical circuits for orientation and direction selectivity. *bioRxiv* **21,** 556795 (2019).

Fig. 1 | XEN cells induce neural tube-like structures in gastruloids. a, Schematic of the culture protocol: at 0 h, 200 cells (150 ESCs and 50 XEN cells) were aggregated; CHIR was added between 48 h and 72 h after cell seeding; cell aggregates were cultured until 96 h. **b**, T and SOX2 expression in aggregates at 96 h (z-projection of whole mount immunostaining). Inset: aggregate resulting from the standard gastruloid protocol (without XEN cells). Scale bars 100 µm. **c**, Average fraction of aggregates showing tubular structures and T staining at 96 h for different starting ratios of ESCs and XEN cells (n=2 experiments, error bars show standard deviation). **d**, SOX2, E-cadherin and N-cadherin immunostaining in sections of 96 h aggregates. Scale bar 50 µm. **e**, T, SOX2, PAX6 and NKX6.1 immunostaining in 96 h aggregates. Scale bars 100 µm. **b, d-e,** Cells nuclei were stained with DAPI.

Fig. 2 | Single-cell RNA-sequencing reveals expression differences between neuruloids and gastruloids. a,**b**, Umap of cells in neuruloids and gastruloids (2 replicates each) colored by cell type based on mapping to *in vivo* data[15]. **c**, Cell type frequencies in neuruloids and gastruloids. **d**, Developmental age of cell types based on mapping to *in vivo* data. **e**, Umap of cells in neuruloids and gastruloids with spike-in cells and XEN derived cells highlighted by color. **f**, *Sox2*, *Pax6*, *Nkx6.1* and *T* log-expression levels indicated by color in umaps of neuruloids. **g**, Gene expression differences between cells classified as spinal cord and all other cells in neuruloids (fold-change vs p-value). Named genes are expressed in the neural tubes according to previous studies (Extended Data Table 1). **h**, Gene expression differences between cells classified as spinal cord in gastruloids and neuruloids (fold-change vs p-value).

Underlined genes are expressed in the dorsal part of the neural tube according to previous studies (Extended Data Table 2).

Fig. 3 | Tubular structures show developmental potential resembling neural tubes *in vivo*. **a,** Live cell imaging of SOX1 expression in gastruloids (top panel) and neuruloids (lower panel) grown with *Sox1*-GFP mESCs (see Supplementary Videos 1-6). The arrows indicate the formation of two SOX1 positive tubes between 72 h and 91 h (tube 1: white arrows, tube 2 yellow arrows). Scale bars 10 µm. **b,** Schematic of the signaling experiments. Neuruloids were treated from 72 h to 96 h, with either BMP pathway inhibitor (BMPi), retinoic acid (RA) or hedgehog pathway agonist (Hh agonist). The neuruloids were then allowed to grow for an additional 48 h before staining. **c,** SOX2, NKX6.1 and PAX6 immunostaining in sections of neuruloids at 144 h, treated with the indicated factors. N = 3 experiments. Scale bars 100 µm. **d,** SOX2 and TUJ1 immunostaining in a section of neuruloid-derived cerebral cortex-like tissue, 8 days after cell seeding (differentiated from neuruloids for 4 days). Scale bar 100 µm. **c-d**, Cell nuclei are stained with DAPI.

Fig. 4 | XEN cells guide symmetry breaking by locally inhibiting primitive streak formation. a, Left, cell types of XEN-derived cells in neuruloids. Cells were classified as gut, parietal endoderm (parietal end.), embryonic VE (visceral end.) or extraembryonic VE (ExE end.). Right, cell types of spiked-in XEN cells. **b**, Gene expression differences between XEN spike-ins and XEN-derived cells in neuruloids (fold-change vs p-value). Orange and pink lines indicate genes with PE-like and VE-like identity, respectively (see Extended Data Table 3). **c**, *Dab2*, *Spink1* and *Fst* expression visualized by single molecule fluorescence *in situ* hybridization (smFISH). Cell nuclei were stained with DAPI. Each diffraction limited dot is a single mRNA molecule. Left, section of a neuruloid at 96 h. Scale bar 50 µm. Right, XEN cells

cultured under standard maintenance conditions (top) and XEN cells treated with CHIR according to the neuruloid protocol (bottom). Scale bars 20 µm. **d**, E-cadherin immunostaining in sections of neuruloids at 96 h. XEN cells were localized by expression of GATA6. Zoom-ins are outlined by dashed boxes 1-3 and shown on the right. **e**, T and SOX2 expression in neuruloids (left) and gastruloids (right) at 72 h (z-projection of whole mount immunostaining). XEN cells were localized by expression of DAB2 and are indicated by a dashed outline. **f**, SOX2 and laminin immunostaining in sections of neuruloids at 96 h. XEN cells were localized by expression of GATA6. A zoom-in is outlined by a dashed box and shown on the right. **g**, T and SOX2 expression in gastruloids grown in XEN-conditioned media at 96 h (z-projection of whole mount immunostaining). **d-g**, Cell nuclei were stained with DAPI. Scale bars 50 µm.

Methods

Experimental methods

Cell culture

All cell lines were routinely cultured in KO DMEM medium (Gibco) supplemented with 10% ES certified FBS (Gibco), 0.1 mM 2-Mercaptoethanol (Sigma-Aldrich), 1 × 100 U/mL penicillin/streptomycin, 1x MEM Non-Essential Amino Acids (Gibco), 2 mM L-glutamine (Gibco), 1000 U/mL mouse LIF (ESGRO). Cells were passaged every other day and replated in tissue-culture treated dishes coated with gelatin. E14 mouse ES cells were provided by Alexander van Oudenaarden. The *Sox1*^{GFPiresPac} mouse ES cell line was created by Mario Stavridis and Meng Li in the group of Austin Smith[34] and provided by Sally Lowell. XEN and XEN-*eGFP* were provided by Christian Schröter[25]. All cell lines were regularly tested for mycoplasma infection. The ES-mCherry-GPI cell line was obtained by introducing a mCherry-

199 GPI transgene in the *Pdgfra*$^{H2B\text{-}GFP}$ cell line, provided by the group of Anna-Katerina
200 Hadjantonakis[35].
201

202 # Differentiation

203 ## Gastruloids

204 The gastruloid differentiation protocol was adapted from van den Brink et al.[1]. ES cells were
205 collected from tissue-culture treated dishes by trypsinization, gentle trituration with a pipet and
206 centrifugation (1200 r.p.m., 3 min). After collection, cells were resuspended in 2 mL of freshly
207 prepared, prewarmed N2B27 medium: DMEM/F12 (Life technologies) supplemented with 0.5
208 × N2 supplement (Gibco), 0.5 × B27 supplement (Gibco), 0.5 mM L-glutamine (Gibco),
209 1 × 100 U/mL penicillin/streptomycin (Gibco), 0.5 × MEM Non-Essential Amino Acids
210 (Gibco), 0.1 mM 2-Mercaptoethanol (Sigma-Aldrich). Cells were counted to determine the cell
211 concentration. For gastruloids, 200 ES cells were seeded in 40 µL of N2B27 in each well of a
212 round-bottom low-adherence 96-well plate. 48 h after seeding, 150 µL of prewarmed N2B27
213 supplemented with 3 µM of GSK3 inhibitor (CHIR99021, Axon Medchem) was added to each
214 well. 72 h after seeding, 150 µL of medium was removed from each well and replaced by 150
215 µL of preheated N2B27. Gastruloids were collected at 96 h after seeding and fixed with 4%
216 paraformaldehyde (PFA, Alfa Aesar) overnight at 4 ºC.
217 For the experiments with gastruloids grown in Geltrex, cell aggregates were collected at 24 h,
218 48 h and 72 h and embedded into LDEV-Free, hESC-Qualified, reduced growth factor Geltrex
219 (Gibco) in culture dishes for the rest of the procedure. Only the gastruloids transferred at 72 h
220 showed robust growth. At 96 h, culture dishes were covered with ice-cold PBS and placed on
221 a shaker at 4 ºC for 10 min. Gastruloids were gently collected by pipetting and washed three
222 times by centrifugation in ice-cold PBS to remove the gel, then fixed with 4% PFA overnight
223 at 4 ºC.

Neuruloids

ES and XEN cells were collected from tissue-culture treated dishes by trypsinization, gentle trituration with a pipet and centrifugation (1200 r.p.m., 3 min). After collection, cells were resuspended in 2 mL of fresh and prewarmed N2B27 medium. Cells were counted to determine cell concentration. For neuruloids, several ratios of XEN and ES cells were tested (1:1, 1:2, 1:3, 1:4, 1:5) and compared with the regular gastruloid condition (0:1). The total number of cells was fixed at 200. Over two separate experiments, the proportion of organoids showing T staining and tubular structures was quantified (total number of embryonic organoids 1:1=179, 1:2=143, 1:3=143, 1:4=140, 0:1=130) and the optimal ratio was determined to be 1:3 (see Fig. 1c and Extended Data Fig. 1a). A total of 200 cells (150 ES cells and 50 XEN cells) was seeded in 40 µL of N2B27 in each well of a round-bottom low-adherence 96-well plate. 48 h after seeding, 150 µL of prewarmed N2B27 supplemented with 3 µM of GSK3 inhibitor (CHIR99021, Axon Medchem) was added to each well. 72 h after seeding, 150 µL of medium was removed from each well and replaced by 150 µL of prewarmed N2B27. Neuruloids were collected at 96 h after seeding and fixed with 4% PFA overnight at 4 ºC.

For the experiment of neuruloids grown without GSK3 inhibitor, cells were seeded as usual. At 48 h, 150 µL of preheated N2B27 was added to each well. At 72 h, 150 µL of medium was removed from each well and replaced by 150 µL of prewarmed N2B27. Neuruloids were collected at 96 h after seeding.

For the smFISH control experiments, XEN cells were seeded at low density in N2B27 medium. At 48 h the medium was replaced by prewarmed N2B27 supplemented with 3 µM of GSK3 inhibitor. 72 h after seeding, the medium was replaced with prewarmed N2B27. Cells were fixed at 96 h with 4% PFA for 1 h at 4 ºC.

Cerebral cortex differentiation

Cerebral cortex-like tissue was created according to a protocol adapted from Lancaster et al.,[21]. Instead of collecting neuruloids at 96 h, the medium was replaced by cerebral organoid differentiation medium: DMEM-F12 (Life technologies), Neurobasal (Gibco), 0.5 × B27 supplement containing vitamin A (Gibco), 0.5 × N2 supplement (Gibco), 2.5 µM/mL Insulin, 2mM L-glutamine (Gibco), 0.5 × MEM-Non-Essential Amino Acids (Gibco), 1 × 100 U/mL penicillin-streptomycin and 0.05 mM 2-Mercaptoethanol (Sigma-Aldrich). At 168 h, aggregates were collected and transferred, with fresh medium, into 10 cm dishes on an orbital shaker installed in the incubator (85 r.p.m.). Aggregates were grown until 192 h (8 days) during which medium was refreshed every other day until collection. Collected aggregates were fixed with 4% PFA for 48 h at 4 ºC.

Signaling experiments

In the signaling experiments with neuruloids, aggregates were treated between 72 h and 96 h with either LDN193189 (BMPi, 100 nM, Reagents Direct), a potent BMP pathway inhibitor, Purmorphamine (1 µM, STEMCELL Technologies), a small molecule agonist of the hedgehog pathway, Retinoic acid (RA, 100 nM, Sigma-Aldrich) or DMSO (0.1% final concentration, Sigma Aldrich) as a vehicle control. For this experiment, the neuruloids were allowed to grow for an additional 48 h before fixation (144 h total growth) and preparation for staining (see Immunostaining).

Immunostaining

Fixation and blocking

After collection, gastruloids and neuruloids were fixed in 4% PFA at 4 °C overnight. Cerebral cortex-like tissue was fixed under the same conditions, but for 48 h. After fixation, samples

were washed three times in washing solution (PBS, 1% bovine serum albumin (BSA)) and incubated at 4 °C in blocking buffer (PBS, 1% BSA, 0.3% Triton-X-100) for a minimum of 16 h. Samples for smFISH were washed 3 times in PBS after fixation and stored in 70% ethanol at 4 °C. To stain E14 cells for pluripotency markers, cells in suspension were fixed for 30 min in 4% PFA at 4 °C, washed three times in washing solution at RT and incubated in blocking buffer for 1 h at 4 °C.

Whole-mount immunolabeling and clearing

Immunolabeling and clearing of gastruloids and neuruloids were based on the protocol described by Dekkers et al.,[36]. Briefly, after fixation and blocking, samples were incubated with primary antibodies at 4 °C overnight on a rolling mixer (30 r.p.m.) in organoid washing buffer (OWB) (PBS, 2% BSA, 0.1% Triton-X-100) supplemented with 0.02% sodium dodecyl sulfate (SDS), referred to as OWB-SDS. The following primary antibodies were used: rat anti-SOX2 (1:200, 14-9811-82, Thermo Fisher Scientific), goat anti-T (1:200, sc-17745, Santa Cruz Biotechnology), goat anti-T (1:100, AF2085, R&D systems), mouse anti-DAB2 (1:100, 610464, BD Biosciences). The next day, samples were washed three times for 2 h in OWB-SDS at RT, followed by incubation with secondary antibodies (donkey anti-goat Alexa Fluor 488 (1:200, A-11055, Thermo Fisher Scientific), donkey anti-rat Alexa Fluor 488 (1:200, A-21208, Thermo Fisher Scientific), donkey anti-goat Alexa Fluor 555 (1:200, A-21432, Thermo Fisher), donkey anti-mouse Alexa Fluor 555 (1:200, A-31570, Thermo Fisher Scientific), chicken anti-rat Alexa Fluor 647 (1:200, A-21472, Thermo Fisher Scientific)) and 4',6-diamidino-2-phenylindole (DAPI, 1 µg/mL, Merck) in OWB-SDS at 4 °C overnight on a rolling mixer (30 r.p.m.), protected from light. Finally, samples were washed three times for 2 h in OWB-SDS at RT. Clearing was performed by incubation in fructose-glycerol clearing solution (60% vol/vol glycerol, 2.5 M fructose) for 20 min at RT. Samples were imaged directly after clearing or stored at 4 °C in the dark.

Cryosectioning and immunolabeling of sections

Prior to cryosectioning, fixed and blocked samples were incubated sequentially in sucrose solutions (10, 20 and 30%) for 30 min (gastruloids and neuruloids) or 2 h (cerebral organoids) at 27 °C, and embedded in optimal cutting temperature (OCT) compound. Samples in OCT were placed on dry ice for rapid freezing, and stored at -80 °C prior to cryosectioning. Samples were cut to cryosections (10 µm thickness) using a cryostat (Thermo Fisher Scientific, USA) and cryosections were placed on poly-L-lysine coated glass slides (Merck). The slides were stored directly at -80 °C. For immunofluorescence staining, slides were thawed and rinsed with PBS for 10 min at RT to dissolve the OCT. Subsequently, slides were incubated overnight at 4 °C with the following primary antibodies diluted in blocking buffer: rat anti-SOX2 (1:200, 14-9811-82, Thermo Fisher Scientific), goat anti-T (1:200, sc-17745, Santa Cruz Biotechnology), mouse anti-N-cadherin (1:200, 33-3900, Thermo Fisher Scientific), rabbit anti-E-cadherin (1:200, 3195, Cell Signaling Technology), rabbit anti-PAX6 (1:100 (cerebral organoids) or 1:200 (gastruloids, neuruloids), 42-6600, Thermo Fisher Scientific), mouse anti-NKX6.1 (1:200, F55A12, Developmental Studies Hybridoma Bank), rabbit anti-NKX6.1 (1:200, HPA036774, Merck), mouse anti-TUJ1 (1:200, 801202, BioLegend), rabbit anti-CD31 (1:50, ab28364, Abcam), rabbit anti-GATA6 (1:200, PA1-104, Thermo Fisher Scientific), goat anti-GATA6 (1:200, AF1700, R&D Systems), rabbit anti-Laminin (1:200, PA1-16730, Thermo Fisher Scientific), mouse anti-OCT4 (1:200, MA1-104, Thermo Fisher Scientific). The next day, the slides were washed twice for 10 min in PBS at RT. Subsequently, the slides were incubated with secondary antibodies (donkey anti-goat Alexa Fluor 488 (1:200, A-11055, Thermo Fisher Scientific), donkey anti-rat Alexa Fluor 488 (1:200, A-21208, Thermo Fisher Scientific), donkey anti-goat Alexa Fluor 555 (1:200, A-21432, Thermo Fisher), donkey anti-mouse Alexa Fluor 555 (1:200, A-31570, Thermo Fisher Scientific), chicken anti-rat Alexa Fluor 647 (1:200, A-21472, Thermo Fisher Scientific), donkey anti-rabbit Alexa Fluor 647

(1:200, A-31573, Thermo Fisher Scientific)) and DAPI (1 µg/mL, Merck) in blocking buffer for 4 h at 4 °C, and washed three times for 10 min at RT. Slides were mounted in ProLong™ Gold Antifade Mountant (Thermo Fisher Scientific) and imaged after 24-48 h.

Immunolabeling of E14 cells

After fixation and blocking, E14 cells were incubated with the following primary antibodies in blocking buffer overnight at 4 °C: rat anti-SOX2 (1:200, 14-9811-82, Thermo Fisher Scientific) and mouse anti-OCT4 (1:200, MA1-104, Thermo Fisher Scientific). The next day, cells were washed three times in washing solution for 5 min at RT and incubated with secondary antibodies (donkey anti-rat Alexa Fluor 488 (1:200, A-21208, Thermo Fisher Scientific) and donkey anti-mouse Alexa Fluor 555 (1:200, A-31570, Thermo Fisher Scientific)) and DAPI (1 µg/mL, Merck) in blocking buffer for 3 h at 4 °C. Finally, the cells were washed three times in washing solution for 5 min at RT and imaged directly.

Single-molecule fluorescence in-situ hybridization (smFISH)

smFISH was performed as described previously[37]. Briefly, samples were fixed with PFA and stored in 70% ethanol, as described above. Custom designed smFISH probes for *Dab2*, *Fst*, *Hhex* and *Spink1* (BioCat, Supplementary Table 2), labeled with Quasar 570, CAL Fluor Red 610, or Quasar 670, were incubated with the samples overnight at 30 °C in hybridization buffer (100 mg/mL dextran sulfate, 25% formamide, 2X SSC, 1 mg/mL E.coli tRNA, 1 mM vanadyl ribonucleoside complex, 0.25 mg/mL BSA; Thermo Fisher Scientific). Samples were washed twice for 30 min at 30 °C with wash buffer (25% formamide, 2X SSC). The wash buffer was supplemented with DAPI (1 µg/mL) in the second wash step. All solutions were prepared with RNAse-free water. Finally, the samples were mounted in ProlongGold (Life Technologies) and imaged when hardened (sections) or immediately (ibidi dishes). All components are from Sigma-Aldrich unless indicated.

Imaging

Fixed and stained samples were imaged on a Nikon Ti-Eclipse epifluorescence microscope equipped with an Andor iXON Ultra 888 EMCCD camera and dedicated, custom-made fluorescence filter sets (Nikon). Primarily, a 10× / 0.3 Plan Fluor DLL objective, a 20× / 0.5 Plan Fluor DLL objective, or a 40× / 1.3 Super Fluor oil-immersion objective (Nikon) were used. To image complete sections of cerebral organoids, multiple adjacent fields of view were acquired and combined using the tiling feature of the NIS Elements software (Nikon). Z-stacks were collected of whole-mount gastruloids and neuruloids with distances of 10 µm between planes. For smFISH measurements, z-stacks were collected with a distance of 0.2 µm between planes in four fluorescence channels (DAPI, Quasar 570, CAL Fluor Red 610, Quasar 670) using a 100× /1.45 Plan Apo Lambda oil (Nikon) objective. To track SOX1 expression in gastruloids and neuruloids during the 24 h growth after the GSK3 inhibitor pulse, 72 h gastruloids and neuruloids grown from the *Sox1*^{GFPiresPac} ES cell line were transferred to a glass-bottom µ-Slide imaging chamber (ibidi) and imaged every 40 min for 24 h, while temperature and CO_2 levels were maintained at 37 °C and 5%, respectively, by a stage top incubator (INUG2-TIZW-SET, Tokai Hit) mounted on the Nikon Ti-Eclipse epifluorescence microscope.

Single-cell RNA-seq library preparation and sequencing

For each replicate, 96 pooled gastruloids and 96 pooled neuruloids were collected from a round-bottomed low-adherence 96-well plate in 15 mL Falcon tubes and pelleted by gentle centrifugation (500 r.p.m. for 2 min). No final aggregate was excluded from the collection. After washing with cold PBS, samples were resuspended in N2B27. Cells were then dissociated by 5 min incubation in TrypLE (Gibco) and gentle trituration with a pipet,

centrifuged and resuspended in 1 mL of cold N2B27. Cells were counted to determine cell number and viability. For the first replicate, ES-mCherry-GPI were spiked in at a frequency of 5%. For the second replicate, E14 cells were collected from culture dishes and incubated for 30 min at 4 ºC with CITE-seq cell hashing[38] antibody Ab_CD15 (1:200) (Biolegend). XEN-*eGFP* were collected from culture plates and incubated for 30 min at 4 ºC with CITE-seq cell hashing antibody Ab_CD140 (1:200) (Biolegend). In the gastruloid sample, labeled E14 cells were spiked in at a frequency of 5%, whereas in the neuruloid sample labeled E14 and XEN-*eGFP* were spiked in, both at a frequency of 5%. High viability of the cells in all samples was confirmed before 10X library preparation. Single-cell RNA-seq libraries were prepared using the Chromium Single Cell 3' Reagent Kit, Version 3 Chemistry (10x Genomics) according to the manufacturer's protocol. CITE-seq libraries were prepared according to the CITE-seq protocol from New York Genome Center version 2019-02-13. Libraries were sequenced paired end on an Illumina Novaseq6000 at 150 base pairs.

Computational methods

Analysis of single-cell RNA-sequencing data

Single-cell RNA-seq data pruning and normalization

Cells with a low number of transcripts were excluded from further analysis based on the histograms in Extended Data Fig. 2a (count < 1300 for replicate 1 of the neuruloid experiment and count < 2300 for the other datasets). Genes expressed in less than 2 cells (across merged replicates) were excluded from further analysis. The final neuruloid dataset contains 14286 genes and 4591 or 6857 cells for replicate 1 or 2, respectively. The gastruloid dataset contains 14384 genes and 4233 or 8363 cells per replicate. The two datasets were normalized using the scran R-package (V 1.10.2[39]). Gene variabilities were calculated (improvedCV2, scran) for each replicate separately, after excluding ribosomal genes [Ribosomal Protein Gene Database,

399 http://ribosome.med.miyazaki-u.ac.jp/], exogenously expressed genes and genes expressing
400 the antibodies used for CITE-seq. The 10% most highly variable genes (HVG) were selected
401 based on variability p-values.

402 **Dimensionality reduction**

403 For each of the two datasets, the two replicates were batch corrected with the fast mutual
404 nearest neighbors (MNN) method implemented in the scran R-package[40], using the union of
405 the 10% HVG of the two replicates and log-transformed normalized counts with d = 120
406 (number of principal components) and k = 50 (number of nearest neighbours). For
407 dimensionality reduction, a uniform manifold approximation and projection (umap) was
408 calculated on the batch corrected data using the R-package umap (V 0.2.3.1[41]) with n = 50,
409 min_dist = 0.7 and using the cosine distance measure.

410 **Identification of spike-in cells**

411 Cells with any expression of mCherry were annotated as ES (mCherry+). The remaining spike-
412 in cells, E14 (CD15+) and XEN spike-in (CD140+) (see Single-cell RNA-seq library
413 preparation and sequencing), could not be determined by the expression level of the antibody
414 alone. We therefore chose to assign spike-ins based on clusters. For each of the two datasets, a
415 shared nearest neighbor graph was constructed from the batch corrected data (see
416 Dimensionality reduction) with scran using k = 20 and d = 30. Louvain clustering was
417 performed on the constructed graphs with the R-package igraph (V1.2.4.1[42]), which resulted in
418 8 clusters for neuruloids and 7 clusters for gastruloids (see Extended Data Fig. 2c). We
419 identified 3 out of the 8 clusters in neuruloids based on literature markers and spike-in gene
420 expression. One cluster out of these three was mainly comprised of mESCs, due to high
421 Ab_CD15 expression and mCherry positive cells. Cells that had an expression of Ab_CD15 >
422 50 and were part of this cluster were considered spiked-in E14 and annotated as E14 (CD15+).
423 The other two clusters were both eGFP positive, where one of them had a higher Ab_CD140

expression and was thus annotated as XEN spike-in (Ab_CD140+). The second cluster was annotated as XEN derived (Ab_CD140-). Similarly, for gastruloids, one of the 7 clusters was comprised of mainly mESCs based on literature markers and spike-in gene expression. Cells that had an expression of Ab_CD15 > 100 and were part of this cluster were considered spiked-in E14 and annotated as E14 (CD15+).

Analysis of cell cycle and stress-related genes

For each of the two datasets, cell cycle analysis was performed with the scran package using the cyclone function[43] on the normalized counts. Cells in G2M phase were distributed evenly across all clusters and thus the clustering was not biased by cell cycle. No other separate cluster that consisted entirely of cell cycle related cells appeared.

For the analysis of stress-related genes, a list of known stress genes[44] was used to calculate the average standardized expression per cell based on normalized counts. Stress-related genes were mainly found within the spike-in cells and there was no other separate cluster that consisted entirely of highly stressed cells.

Mapping to *in vivo* datasets

Our datasets were mapped to three different *in vivo* datasets.

Pijuan-Sala et al. dataset

The Pijuan-Sala et al. dataset[15], which was downloaded from https://content.cruk.cam.ac.uk/jmlab/atlas_data.tar.gz, consists of 9 timepoints from E6.5 to E8.5. The data was normalized by size factors provided by the authors. Cells with no cell type assignment were excluded from further analysis. The 10% HVG were calculated (improvedCV2, scran package) on the remaining cells excluding sex genes, similar to Pijuan-Sala et al.'s method. Cells in the "mixed_gastrulation" cluster were also excluded. MNN mapping was applied to log-transformed normalized counts of the 10% HVG. First, *in vivo* timepoints were mapped to each other in decreasing order. Then, each of our four datasets was

mapped separately to the combined Pijuan-Sala et al. dataset (MNN method with d = 120, k = 50). K-nearest-neighbor (knn) assignment was performed in the batch corrected principal component space. For each cell in our datasets, the 50 nearest neighbors in the *in vivo* dataset, based on Euclidean distances, were calculated. Each cell was assigned the most abundant cell type within the knn, if certain distance and confidence score conditions were met. This confidence score was calculated for each cell as the number of the most abundant cell type divided by the total number of neighbors (k=50). A cell was annotated as "Not assigned" if either, the average distance to its nearest neighbor exceeded a certain threshold (determined by the long tail of the histogram of average distances for each of our datasets separately) or the assignment had a confidence score less than 0.5. Additionally, we placed cells in "Not assigned" if they were assigned to clusters with less than 10 cells, or to the cluster "Blood progenitors 2" (because this cluster did not show distinct expression of known literature markers). This resulted in 22 assigned clusters for neuruloids and 15 assigned clusters for gastruloids. For each cell in our dataset we calculated the average and the standard deviation of the developmental age of the knn.

Nowotschin et al. dataset

The Nowotschin et al. dataset[23], which was downloaded from https://endoderm-explorer.com/, consists of 6 timepoints from E3.5 to E8.75. The data was normalized (scran) and the 10% HVG were calculated (improvedCV2, scran package). First, MNN was applied to the Nowotschin et al. dataset in increasing order of the timepoints (using log-transformed normalized counts of the 10% HVG, d = 150, k =50). Then, XEN cells from our neuruloid dataset (XEN spike-ins (CD140+) and XEN derived (CD140-)) were mapped to the MNN-corrected Nowotschin et al. dataset. Knn assignment was performed as described above and resulted in 7 assigned clusters.

Delile et al. dataset

The Delile et al. dataset[45], which was downloaded from https://github.com/juliendelile/MouseSpinalCordAtlas, consists of 5 timepoints from E9.5 to E13.5. Cells that had a cell type assignment of "Null" or "Outlier" were excluded from further analysis. The data was normalized (scran) and the 10% HVG were calculated. First, MNN was applied to the Delile et al. dataset in order of increasing timepoints (log-transformed normalized counts of the 10% HVG, d = 120, k =50). Then, we mapped neural-like cells (Cells annotated as "Neural crest", "NMP", "Forebrain/Midbrain/Hindbrain", "Rostral neurectoderm", "Caudal neuroectoderm" and "Spinal cord", without applying a cutoff for distance and confidence score.) to the MNN corrected Delile et al. dataset separately for each of our replicates. Knn assignment was performed as described above and resulted in 3 clusters for neuruloids and 3 clusters for gastruloids.

Differential expression analysis

For the differential expression test between "spike-in XENs" and "XENs in neuruloids" a Welch t-test (implemented in findMarkers, scran R package) was conducted on the normalized log-transformed counts. The test was performed on neuruloids from replicate 2. "spike-in XENs" were chosen as the 100 cells with highest Ab_CD140 expression and "XENs in neuruloids" were the 100 cells with lowest Ab_CD140 expression within the XEN identified cells.

For the differential expression test between neuruloids and gastruloids, a negative binomial regression was performed (R package edgeR V 3.24.3[46]). Based on the knn assignment to the Pijuan-Sala et al. dataset, all cells annotated as "Spinal cord" were extracted from our four datasets (in neuruloids 859 cells in replicate 1 and 166 cells in replicate 2, in gastruloids 2071 cells in replicate 1 and 1882 cells in replicate 2). Raw counts were used for the regression with these four subsets as dummy variables and a variable corresponding to the total number of

counts per cell. P-values were obtained for the contrast between neuruloids and gastruloids using the average regression coefficients among variables of both replicates.

Similarly, for the differential expression test of the "Spinal cord" in neuruloids, a negative binomial regression was used. Cells were excluded from the test if either their cell type occurred in less than 10 cells per replicate, or if the cells were annotated as "Not assigned", leaving a total of 13 cell types (7742 cells) to be considered. For each cell type and each replicate a dummy variable was created and a variable corresponding to the total number of counts per cell. Then, p-values were obtained for the contrast between the average regression coefficients of the two replicates of the "Spinal cord" cluster and the average regression coefficients of all other variables considered in the test.

For all differential expression tests p-values were adjusted for multiple hypothesis testing with the Benjamini-Hochberg method.

Image analysis

Image stacks of whole-mount immunostained gastruloids and neuruloids, and images of immunostained sections were pre-processed by background subtraction (rolling ball, radius: 50 pixels = 65 µm (10× objective), 32 µm (20× objective) or 16 µm (40× objective)) in the channels that showed autofluorescent background using ImageJ [47]. When background subtraction in images of sections did not result in proper removal of autofluorescent background signal, the Enhance Local Contrast (CLAHE) tool was used in ImageJ [47]. smFISH image stacks were pre-processed by applying a Laplacian of a Gaussian filter ($\sigma = 1$) over the smFISH channels using scikit-image (v0.16.1) [48]. For all image stacks, a maximum projection was used to obtain a 2D representation. To show a single object per image, images were cropped around the object of interest.

Data availability

The single-cell RNA sequencing datasets generated in this study are available in the Gene Expression Omnibus repository, GSE141530.

Code availability

Custom R and python code used to analyze the data is available from the authors upon request.

34. Ying, Q.-L., Stavridis, M., Griffiths, D., Li, M. & Smith, A. Conversion of embryonic stem cells into neuroectodermal precursors in adherent monoculture. *Nature Biotechnology* **21,** 183–186 (Nature Publishing Group, 2003).

35. Artus, J., Panthier, J.-J. & Hadjantonakis, A.-K. A role for PDGF signaling in expansion of the extra-embryonic endoderm lineage of the mouse blastocyst. *Development* **137,** 3361–3372 (2010).

36. Dekkers, J. F. *et al.* High-resolution 3D imaging of fixed and cleared organoids. *Nat Protoc* **14,** 1756–1771 (2019).

37. Semrau, S. *et al.* FuseFISH: robust detection of transcribed gene fusions in single cells. *Cell Reports* **6,** 18–23 (2014).

38. Stoeckius, M. *et al.* Simultaneous epitope and transcriptome measurement in single cells. *Nature Methods* **14,** 865–868 (2017).

39. Lun, A. T. L., Bach, K. & Marioni, J. C. Pooling across cells to normalize single-cell RNA sequencing data with many zero counts. *Genome Biol.* **17,** 75–14 (2016).

40. Haghverdi, L., Lun, A. T. L., Morgan, M. D. & Marioni, J. C. Batch effects in single-cell RNA-sequencing data are corrected by matching mutual nearest neighbors. *Nature Biotechnology* **36,** 421–427 (2018).

41. McInnes, L., Healy, J. & Melville, J. UMAP: Uniform Manifold Approximation and Projection for Dimension Reduction. (2018).

42. Blondel, V. D., Guillaume, J.-L., Lambiotte, R. & Lefebvre, E. Fast unfolding of communities in large networks. (2008). doi:10.1088/1742-5468/2008/10/P10008

43. Scialdone, A. *et al.* Computational assignment of cell-cycle stage from single-cell transcriptome data. *Methods* **85,** 54–61 (2015).

44. van den Brink, S. C. *et al.* Single-cell sequencing reveals dissociation-induced gene expression in tissue subpopulations. *Nature Methods* **14,** 935–936 (2017).

45. Delile, J. *et al.* Single cell transcriptomics reveals spatial and temporal dynamics of gene expression in the developing mouse spinal cord. *Development* **146,** dev.173807 (2019).

46. Robinson, M. D., McCarthy, D. J. & Smyth, G. K. edgeR: a Bioconductor package for differential expression analysis of digital gene expression data. *Bioinformatics* **26,** 139–140 (2010).

47. Schneider, C. A., Rasband, W. S. & Eliceiri, K. W. NIH Image to ImageJ: 25 years of image analysis. *Nature Methods* **9,** 671–675 (2012).

48. van der Walt, S. *et al.* scikit-image: image processing in Python. *PeerJ* **2,** e453 (2014).

Acknowledgements

We are thankful to Alfonso Martinez Arias for insightful discussions and feedback on the manuscript. We acknowledge Anna-Katerina Hadjantonakis for helpful input at various stages of the project. N. B.-C., M. M., P. v.d. B., M. F. and S.S. were supported by the Netherlands Organisation for Scientific Research (NWO/OCW, www.nwo.nl), as part of the Frontiers of

Nanoscience (NanoFront) program. E.A. acknowledges support by a Stichting voor Fundamenteel Onderzoek der Materie (FOM, www.nwo.nl) projectruimte grant (16PR1040). M.H. acknowledges support by a Netherlands Organisation for Scientific Research (NWO/OCW, www.nwo.nl) VIDI grant (016.Vidi.189.007). This work was carried out on the Dutch national e-infrastructure with the support of SURF Cooperative. The funders had no role in study design, data collection and analysis, decision to publish, or preparation of the manuscript.

Author contributions

N.B.-C., E.A. and M.H. cultured gastruloids and neuruloids. N.B-C., E.A. and M.H. performed signaling experiments and immunostaining and analyzed the resulting images, N.B-C. prepared samples for single-cell RNA sequencing and interpreted the sequencing data, M.M. performed the computational analysis of the single-cell RNA sequencing data, P.v.d.B. contributed to the computational analysis of single-cell RNA sequencing data and carried out the smFISH measurements, M.F. supported all experiments and performed all cryosectioning, N.B.-C., M. M., E.A., P.v.d.B. and M.H. produced figures, N.B.-C., M. M., E.A., P.v.d.B., M.H. and M.F. contributed to the manuscript, T.I., S.T. and S.S. conceived the study and acquired funding. S.S. interpreted the data and wrote the manuscript. All authors discussed the results and commented on the manuscript at all stages.

Competing interest

The authors declare no competing interests.

Supplementary data

See SI_Guide.doc

Correspondence and requests for materials

Should be addressed to S.S., S.T., T.I., or M.H.

Extended data Fig. 1 | Optimization and characterisation of neuruloids. a, SOX2 (neural progenitors-like cells) and T (primitive streak-like cells) expression in gastruloids and neuruloids with different starting ratio of ES and XEN cells (z-projection of whole mount immunostaining). Scale bars 100 μm. **b**, SOX2 and OCT4 expression (immunostaining) in sections of neuruloids at 96 h (left, scale bars 100 μm) and cultured ESCs (right, scale bars 10 μm). **a-b,** Cells nuclei were stained with DAPI.

Extended data Fig. 2 | Single-cell RNA-seq resolves cell type diversity in neuruloids and gastruloids. a, Upper, number of detected genes per cell in each replicate; the blue line indicates a quality control threshold for neuruloids from replicate 1 and the black line for the remaining datasets. Lower, total expression per cell for each dataset. **b**, Umap of cells in neuruloids and gastruloids, colored by replicate. **c**, Umap of cells in neuruloids and gastruloids, colored by Louvain clustering. The encircled clusters contain the spiked-in cells. **d**, Left, average G2M scores for each cell type. Right, umaps of cells in neuruloids and gastruloids colored by G2M score. **e**, Left, average standardized expression of stress-related genes in spike-in cells. Middle, expression of stress-related genes by cell type. Right, umaps of cells in neuruloids and gastruloids with expression of stress-related genes indicated by color. **f**, Umap of Pijuan-Sala et al. dataset with cell types indicated by color. **g**, MNN mapping of neuruloid cells from replicate 2 (bright colors) to the Pijuan-Sala et al. dataset (dim colors), as an example for the mapping procedure. **h**, Cell type frequencies for each replicate in neuruloids and gastruloids resulting from knn assignments based on the mapping in (g). **i**, Differences between relative frequencies of cell types in neuruloids and gastruloids.

Extended data Fig. 3 | Expression of literature markers. Heat map of standardized expression of genes associated with mouse embryonic development in neuruloids and gastruloids. References describing the *in vivo* expression of the genes are given in Supplementary Table 1.

Extended data Fig. 4 | Neural tube-like cells exhibit dorsal characteristics.

a, Expression of *Sox2*, *Pax6* and *Nkx6.1* in neuruloids, as measured by single-cell RNA-seq. **b**, Left, umap of the cells in the Delile et al. dataset colored by cell type. Right, MNN mapping of cells classified as "spinal cord" in replicate 2 neuruloids (bright colors) to the Delile et al. dataset (dim colors), as an example of the mapping procedure. **c**, Umap of cells in neuruloids with log expression of *Bmp2* and *Bmp4* indicated by color.

Extended data Fig. 5 | Neuruloid derived cerebral cortex-like tissue expresses PAX6 and CD31. Immunostaining in sections of cerebral cortex-like tissue differentiated from neuruloids at 8 days after cell seeding. **a**, TUJ1, SOX2 (top) and PAX6 (bottom). The dashed box highlights layered, cortex-like organization adjacent to a ventricle-like cavity. **b,** TUJ1, SOX2 and CD31. Zoom-ins show clusters of CD31-positive cells. **a, b** Cells nuclei were stained with DAPI. Scale bars 100µm.

Extended data Fig. 6 | XEN-derived cells are visceral endoderm-like in neuruloids.

a, **b**, Umaps of the Pijuan-Sala or Nowotschin dataset, respectively. XEN spike-ins and XEN-derived cells from neuruloids replicate 2 (bright colors) are mapped to the *in vivo* datasets (dim colors). Framed cell types correspond to the ones on which XEN cells mapped. **c**, Cell type frequencies of XEN spike-ins and XEN derived cells in neuruloids, resulting from knn

assignments based on the mapping in **(b)**. **d,** *Dab2*, *Fst* and *Hhex* expression visualized by single molecule fluorescence *in situ* hybridization (smFISH). Cell nuclei were stained with DAPI. Each diffraction limited dot is a single mRNA molecule. Left, section of a neuruloid at 96 h. Scale bar 50 µm. Right, XEN cells cultured under standard maintenance conditions (top) and XEN cells treated with CHIR according to the neuruloid protocol (bottom). Scale bars 20 µm.

Extended data Fig. 7 | XEN cells induce stratified epithelium and lumen formation

a, Left, umap of cells in neuruloids with XEN-derived cells colored by cell type (gut, parietal endoderm (parietal end.), embryonic VE (visceral end.) or extraembryonic VE (ExE end.)). Mid-right, umap of cells in neuruloids colored by log expression of Fibronectin (*Fn*), Laminin alpha 1 (*Lama1*) and Laminin beta 1 (*Lamb1*). A violin plot of log expression in XEN-derived cell types is shown below the umap for each gene. **b**, SOX2 and GATA6 immunostaining in sections of gastruloids grown in Geltrex at 96 h. **c**, SOX2 immunostaining in sections of neuruloids grown without CHIR. No specific T staining could be detected (data not shown). XEN cells were localized by expression of GATA6. **b**, **c**, Cell nuclei were stained with DAPI. Scale bars 50 µm.

Extended Data Table 1 | Genes differentially expressed between spinal cord-like cells and the other cells types in neuruloids.

Extended Data Table 2 | Genes differentially expressed between spinal cord-like cells in neuruloids and gastruloids.

Extended data Table 3 | Genes differentially expressed between XEN-derived cells in neuruloids and cultured XEN cells.

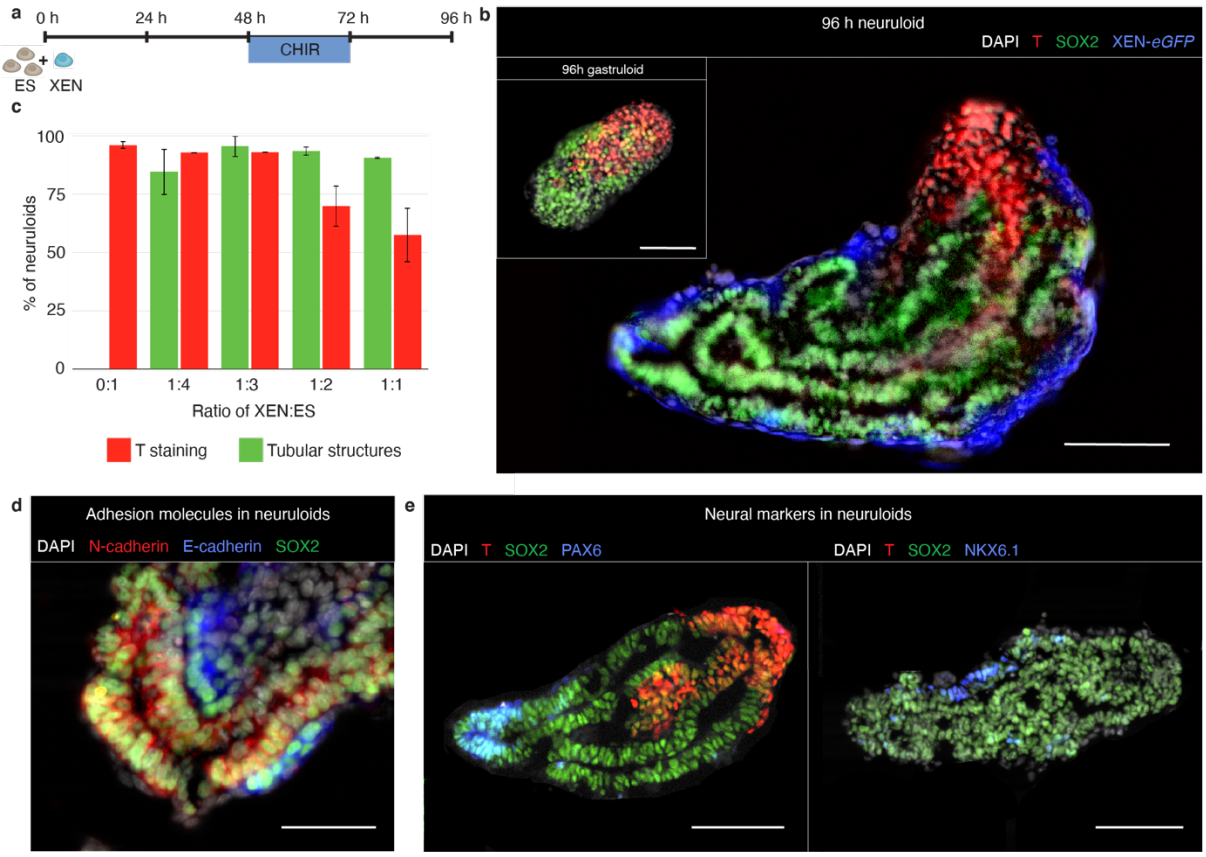

Fig. 1 | XEN cells induce neural tube-like structures in gastruloids. a, Schematic of the culture protocol: at 0 h, 200 cells (150 ESCs and 50 XEN cells) were aggregated; CHIR was added between 48 h and 72 h after cell seeding; cell aggregates were cultured until 96 h. **b**, T and SOX2 expression in aggregates at 96 h (z-projection of whole mount immunostaining). Inset: aggregate resulting from the standard gastruloid protocol (without XEN cells). Scale bars 100 µm. **c**, Average fraction of aggregates showing tubular structures and T staining at 96 h for different starting ratios of ESCs and XEN cells (n=2 experiments, error bars show standard deviation). **d**, SOX2, E-cadherin and N-cadherin immunostaining in sections of 96 h aggregates. Scale bar 50 µm. **e**, T, SOX2, PAX6 and NKX6.1 immunostaining in 96 h aggregates. Scale bars 100 µm. **b, d-e,** Cells nuclei were stained with DAPI.

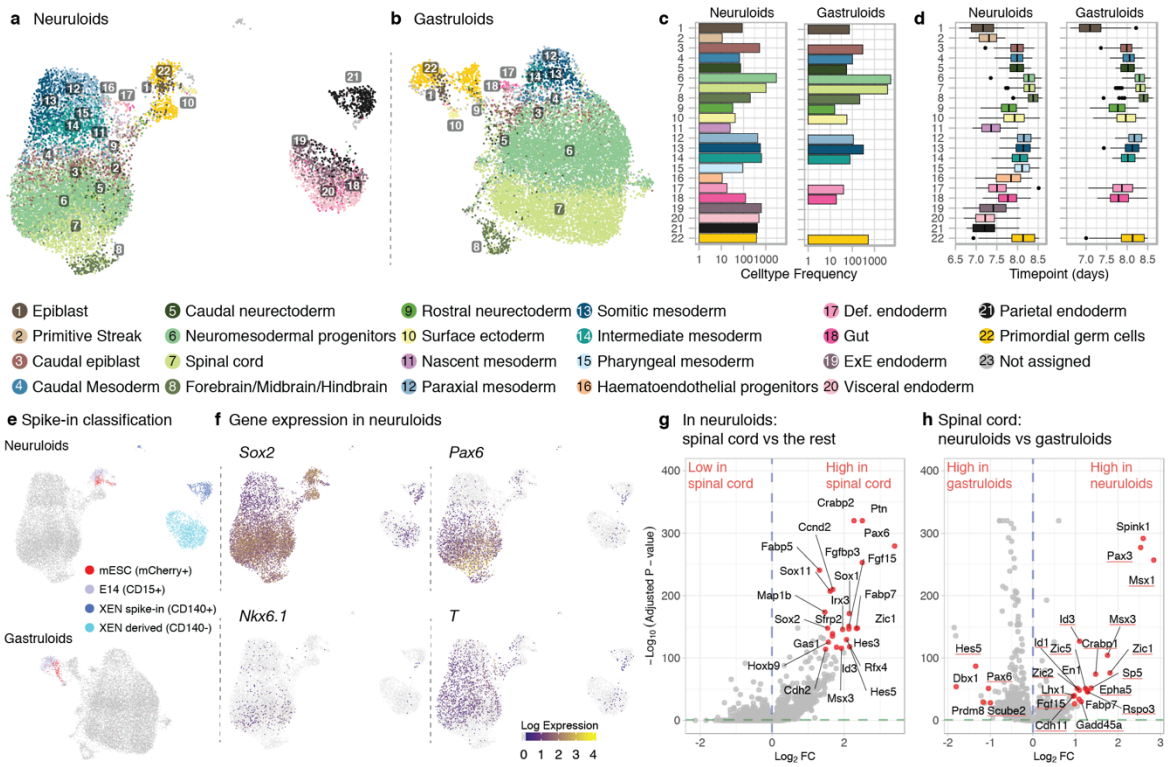

Fig. 2 | Single-cell RNA-sequencing reveals expression differences between neuruloids and gastruloids. a,**b**, Umap of cells in neuruloids and gastruloids (2 replicates each) colored by cell type based on mapping to *in vivo* data[15]. **c**, Cell type frequencies in neuruloids and gastruloids. **d**, Developmental age of cell types based on mapping to *in vivo* data. **e**, Umap of cells in neuruloids and gastruloids with spike-in cells and XEN derived cells highlighted by color. **f**, *Sox2*, *Pax6*, *Nkx6.1* and *T* log-expression levels indicated by color in umaps of neuruloids. **g**, Gene expression differences between cells classified as spinal cord and all other cells in neuruloids (fold-change vs p-value). Named genes are expressed in the neural tubes according to previous studies (Extended Data Table 1). **h**, Gene expression differences between cells classified as spinal cord in gastruloids and neuruloids (fold-change vs p-value). Underlined genes are expressed in the dorsal part of the neural tube according to previous studies (Extended Data Table 2).

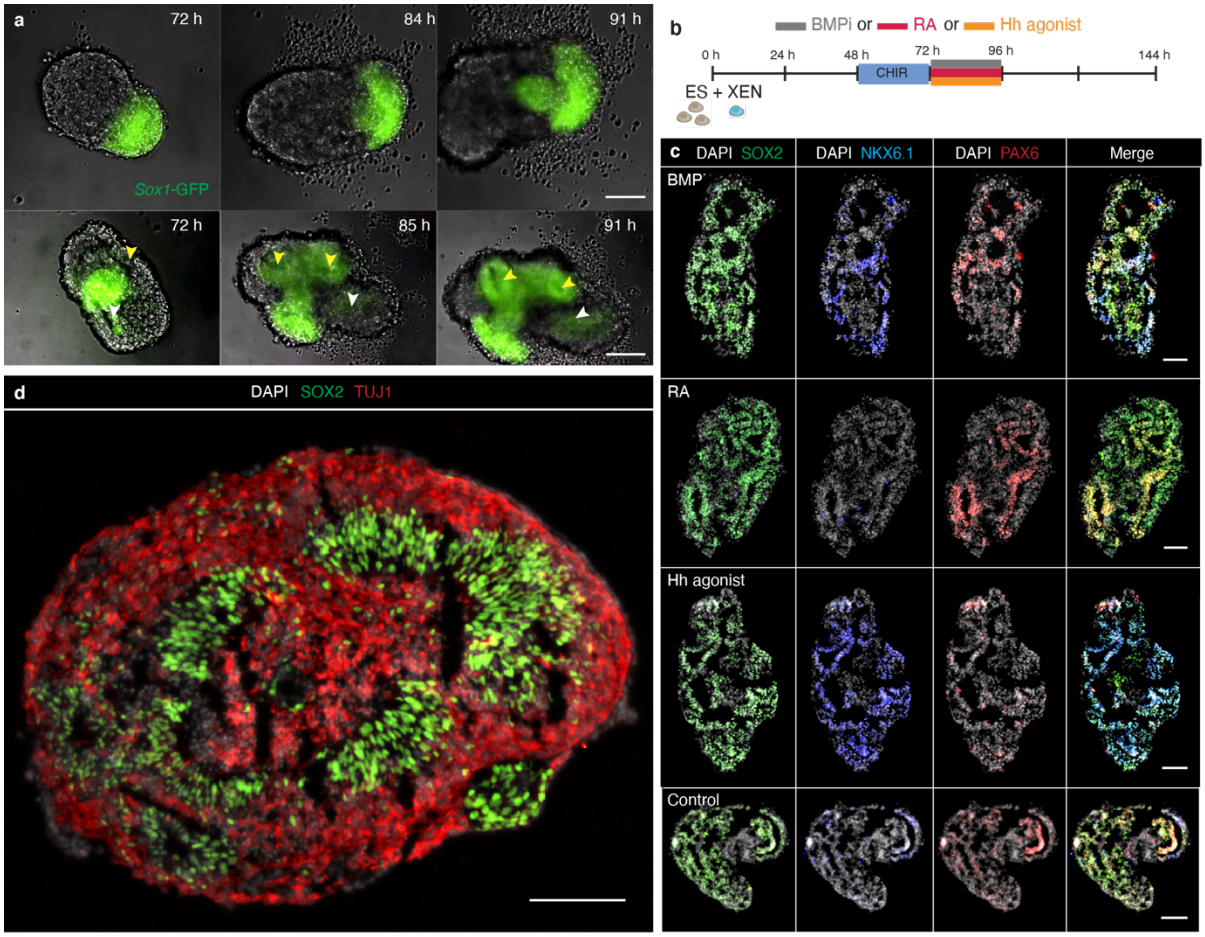

Fig. 3 | Tubular structures show developmental potential resembling neural tubes *in vivo*.

a, Live cell imaging of SOX1 expression in gastruloids (top panel) and neuruloids (lower panel) grown with *Sox1*-GFP mESCs (see Supplementary Videos 1-6). The arrows indicate the formation of two SOX1 positive tubes between 72 h and 91 h (tube 1: white arrows, tube 2 yellow arrows). Scale bars 10 µm. **b,** Schematic of the signaling experiments. Neuruloids were treated from 72 h to 96 h, with either BMP pathway inhibitor (BMPi), retinoic acid (RA) or hedgehog pathway agonist (Hh agonist). The neuruloids were then allowed to grow for an additional 48 h before staining. **c,** SOX2, NKX6.1 and PAX6 immunostaining in sections of neuruloids at 144 h, treated with the indicated factors. N = 3 experiments. Scale bars 100 µm. **d,** SOX2 and TUJ1 immunostaining in a section of neuruloid-derived cerebral cortex-like tissue, 8 days after cell seeding (differentiated from neuruloids for 4 days). Scale bar 100 µm. **c-d**, Cell nuclei are stained with DAPI.

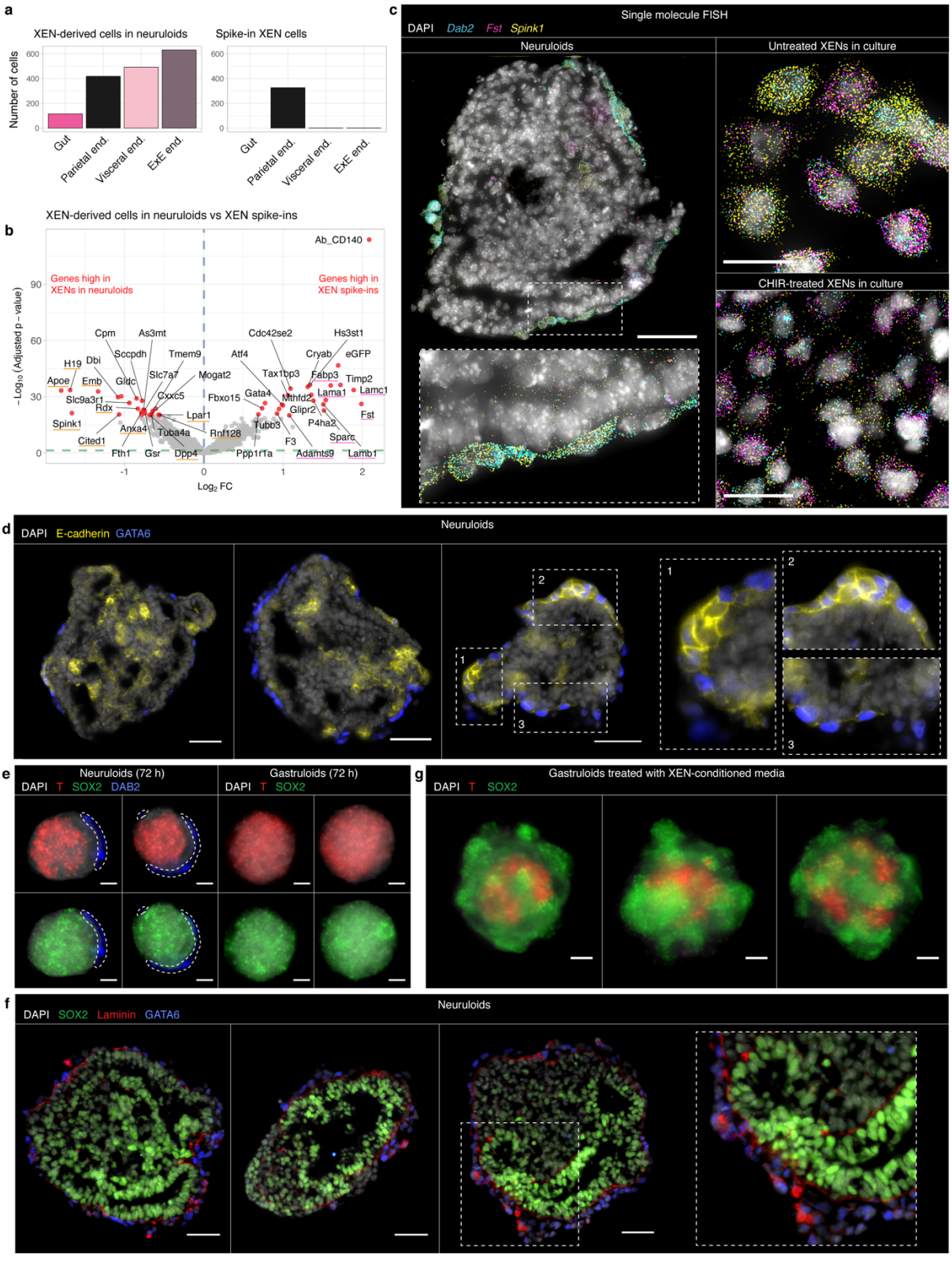

Fig. 4 | XEN cells guide symmetry breaking by locally inhibiting primitive streak formation. a, Left, cell types of XEN-derived cells in neuruloids. Cells were classified as gut, parietal endoderm (parietal end.), embryonic VE (visceral end.) or extraembryonic VE (ExE end.). Right, cell types of spiked-in XEN cells. **b**, Gene expression differences between XEN spike-ins and XEN-derived cells in neuruloids (fold-change vs p-value). Orange and pink lines indicate genes with PE-like and VE-like identity, respectively (see Extended Data Table 3). **c**, *Dab2*, *Spink1* and *Fst* expression visualized by single molecule fluorescence *in situ* hybridization (smFISH). Cell nuclei were stained with DAPI. Each diffraction limited dot is a single mRNA molecule. Left, section of a neuruloid at 96 h. Scale bar 50 µm. Right, XEN cells cultured under standard maintenance conditions (top) and XEN cells treated with CHIR according to the neuruloid protocol (bottom). Scale bars 20 µm. **d**, E-cadherin immunostaining in sections of neuruloids at 96 h. XEN cells were localized by expression of GATA6. Zoom-ins are outlined by dashed boxes 1-3 and shown on the right. **e**, T and SOX2 expression in neuruloids (left) and gastruloids (right) at 72 h (z-projection of whole mount immunostaining). XEN cells were localized by expression of DAB2 and are indicated by a dashed outline. **f**, SOX2 and laminin immunostaining in sections of neuruloids at 96 h. XEN cells were localized by expression of GATA6. A zoom-in is outlined by a dashed box and shown on the right. **g**, T and SOX2 expression in gastruloids grown in XEN-conditioned media at 96 h (z-projection of whole mount immunostaining). **d-g**, Cell nuclei were stained with DAPI. Scale bars 50 µm.

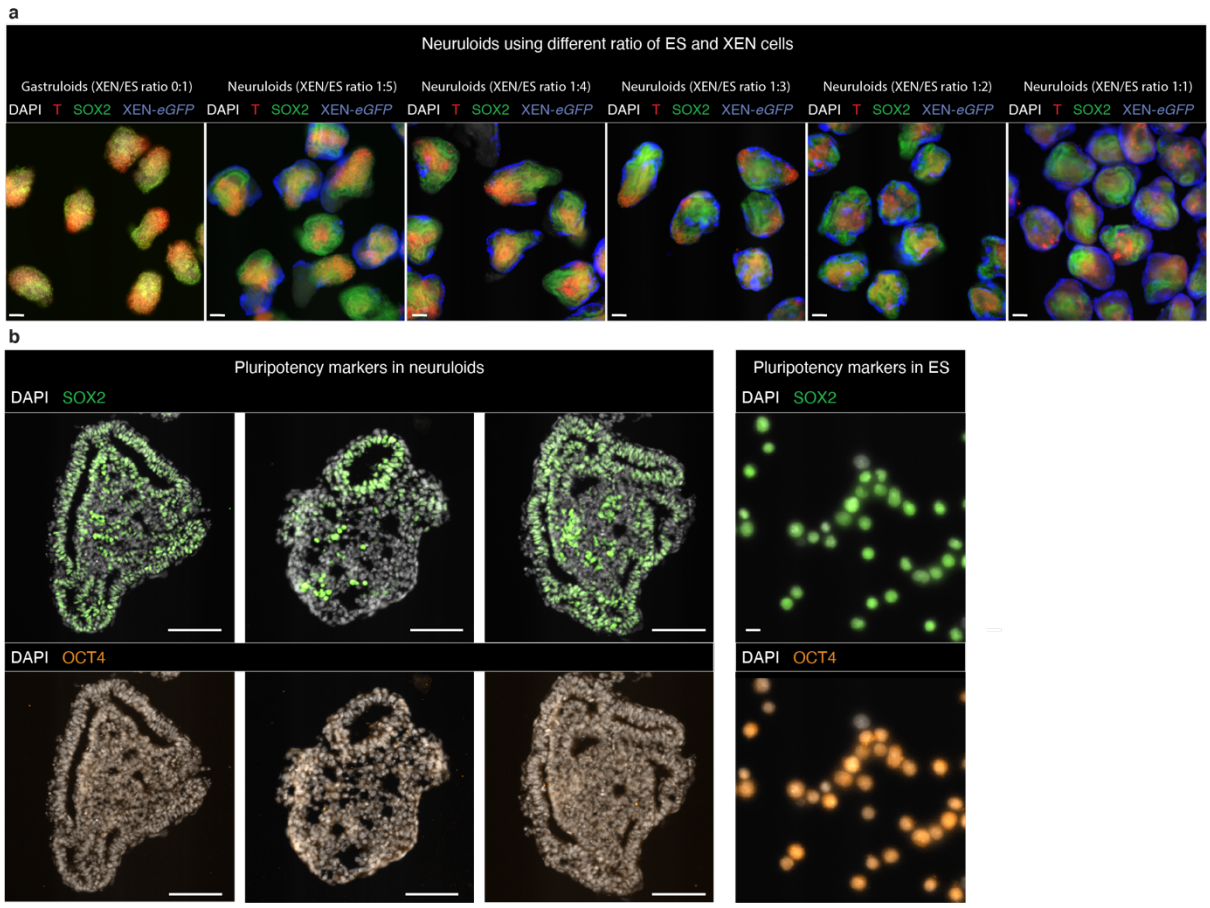

Extended data Fig. 1 | Optimization and characterisation of neuruloids. a, SOX2 (neural progenitors-like cells) and T (primitive streak-like cells) expression in gastruloids and neuruloids with different starting ratio of ES and XEN cells (z-projection of whole mount immunostaining). Scale bars 100 µm. **b**, SOX2 and OCT4 expression (immunostaining) in sections of neuruloids at 96 h (left, scale bars 100 µm) and cultured ESCs (right, scale bars 10 µm). **a-b,** Cells nuclei were stained with DAPI.

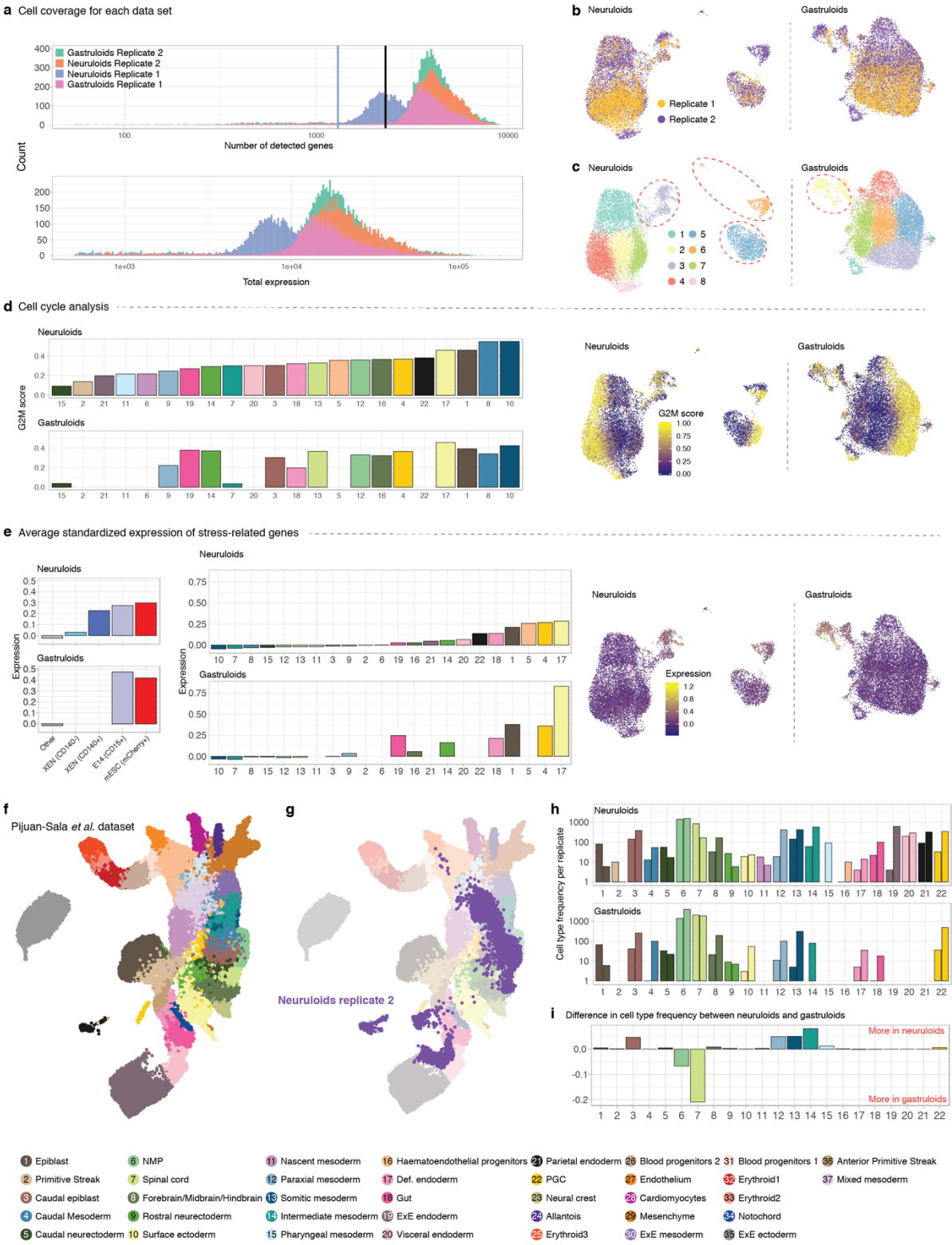

Extended data Fig. 2 | Single-cell RNA-seq resolves cell type diversity in neuruloids and gastruloids. **a**, Upper, number of detected genes per cell in each replicate; the blue line indicates a quality control threshold for neuruloids from replicate 1 and the black line for the remaining datasets. Lower, total expression per cell for each dataset. **b**, Umap of cells in neuruloids and gastruloids, colored by replicate. **c**, Umap of cells in neuruloids and gastruloids, colored by Louvain clustering. The encircled clusters contain the spiked-in cells. **d**, Left, average G2M scores for each cell type. Right, umaps of cells in neuruloids and gastruloids colored by G2M score. **e**, Left, average standardized expression of stress-related genes in spike-in cells. Middle, expression of stress-related genes by cell type. Right, umaps of cells in neuruloids and gastruloids with expression of stress-related genes indicated by color. **f**, Umap of Pijuan-Sala et al. dataset with cell types indicated by color. **g**, MNN mapping of neuruloid cells from replicate 2 (bright colors) to the Pijuan-Sala et al. dataset (dim colors), as an example for the mapping procedure. **h**, Cell type frequencies for each replicate in neuruloids and gastruloids resulting from knn assignments based on the mapping in (g). **i**, Differences between relative frequencies of cell types in neuruloids and gastruloids.

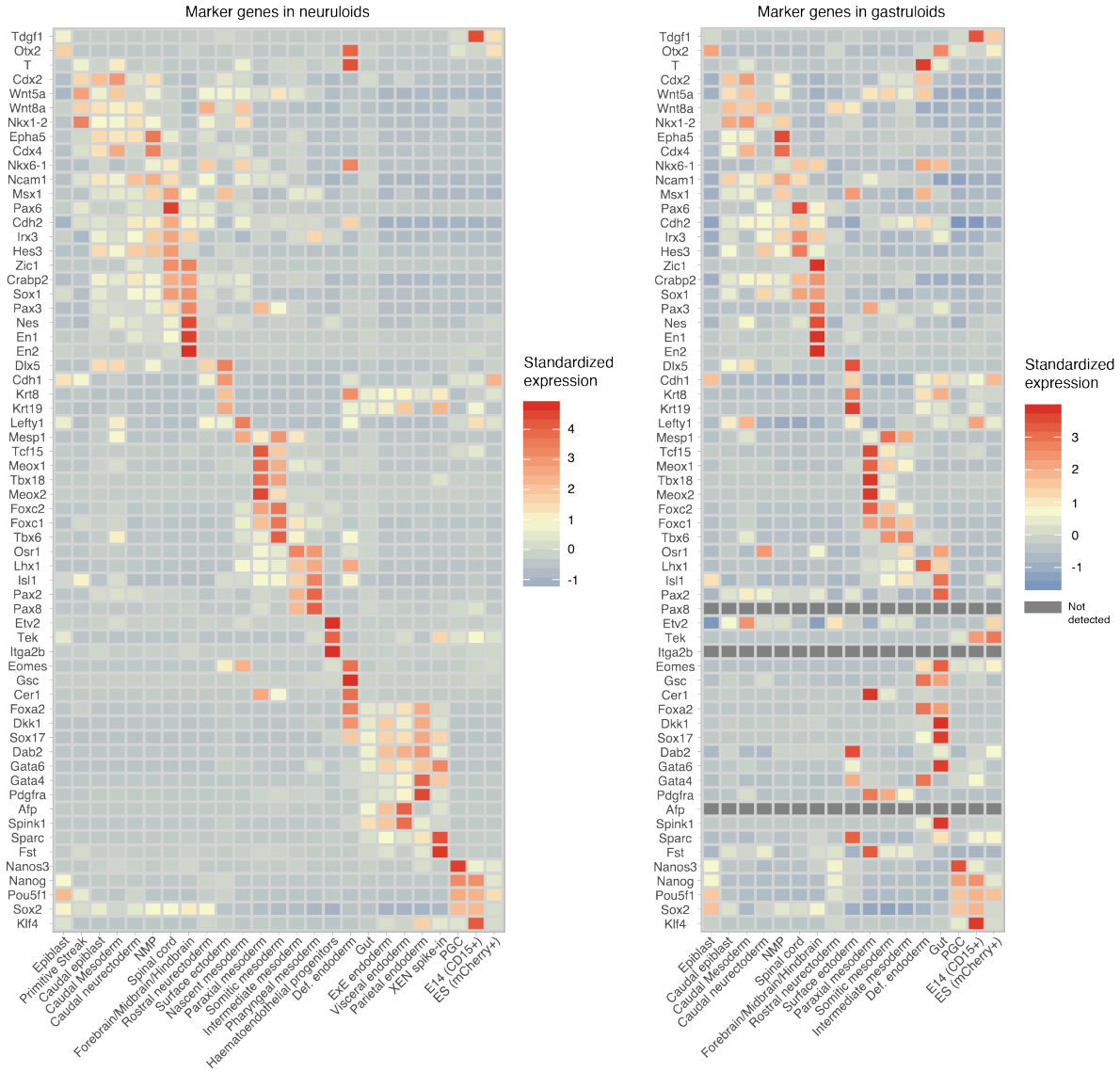

Extended data Fig. 3 | Expression of literature markers. Heat map of standardized expression of genes associated with mouse embryonic development in neuruloids and gastruloids. References describing the *in vivo* expression of the genes are given in Supplementary Table 1.

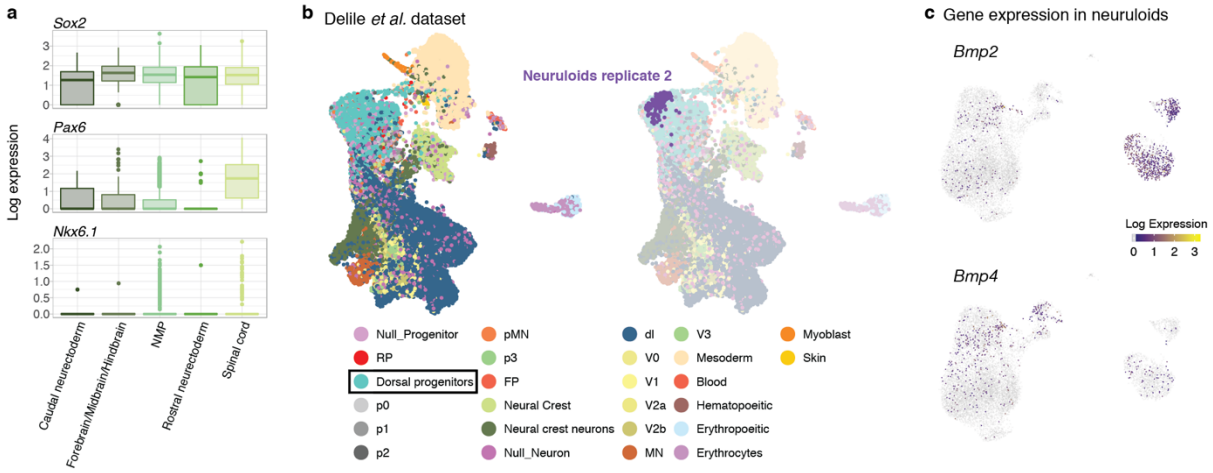

Extended data Fig. 4 | Neural tube-like cells exhibit dorsal characteristics.

a, Expression of *Sox2*, *Pax6* and *Nkx6.1* in neuruloids, as measured by single-cell RNA-seq. **b**, Left, umap of the cells in the Delile et al. dataset colored by cell type. Right, MNN mapping of cells classified as "spinal cord" in replicate 2 neuruloids (bright colors) to the Delile et al. dataset (dim colors), as an example of the mapping procedure. **c**, Umap of cells in neuruloids with log expression of *Bmp2* and *Bmp4* indicated by color.

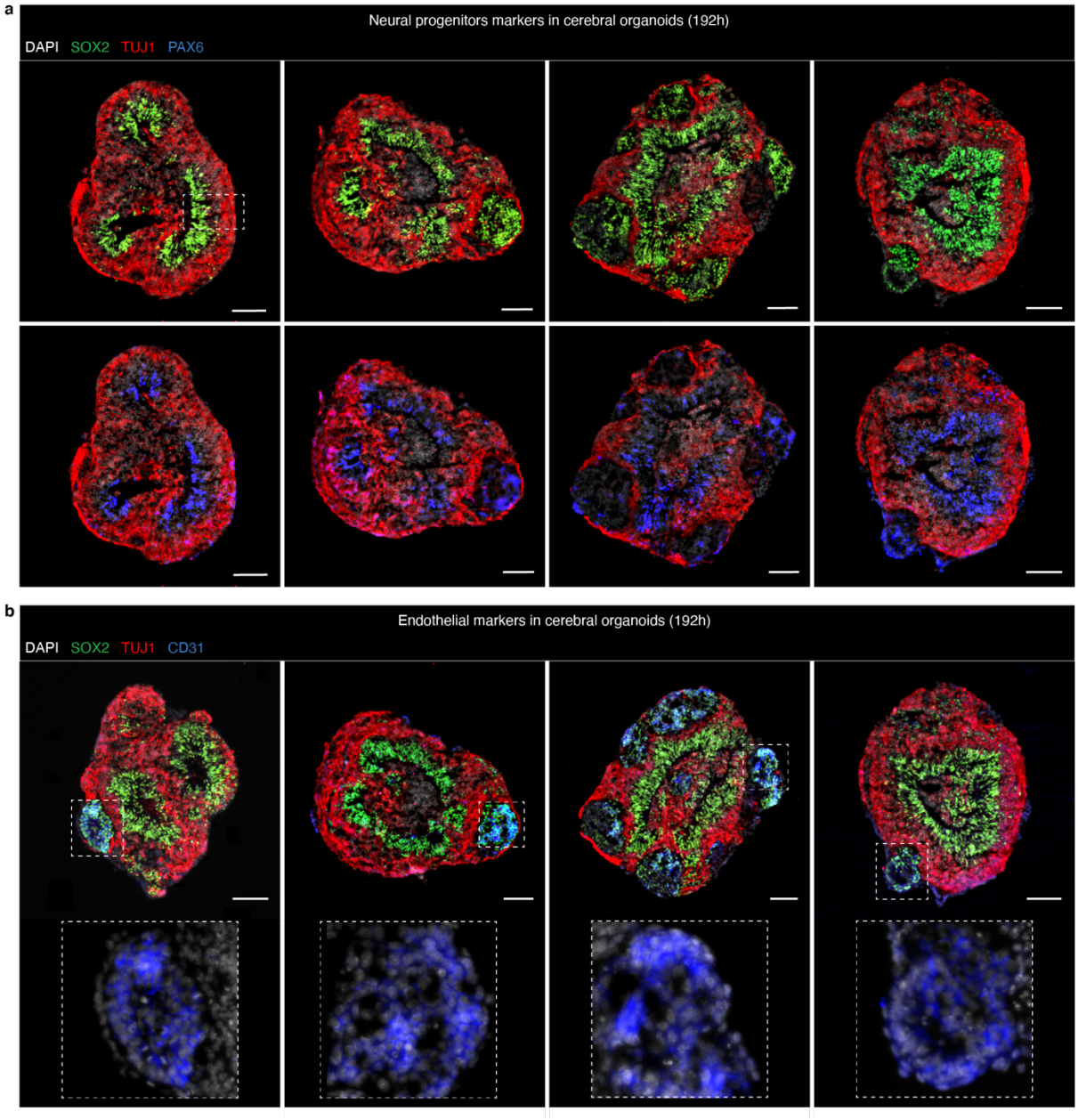

Extended data Fig. 5 | Neuruloid derived cerebral cortex-like tissue expresses PAX6 and CD31. Immunostaining in sections of cerebral cortex-like tissue differentiated from neuruloids at 8 days after cell seeding. **a**, TUJ1, SOX2 (top) and PAX6 (bottom). The dashed box highlights layered, cortex-like organization adjacent to a ventricle-like cavity. **b,** TUJ1, SOX2 and CD31. Zoom-ins show clusters of CD31-positive cells. **a, b** Cells nuclei were stained with DAPI. Scale bars 100µm.

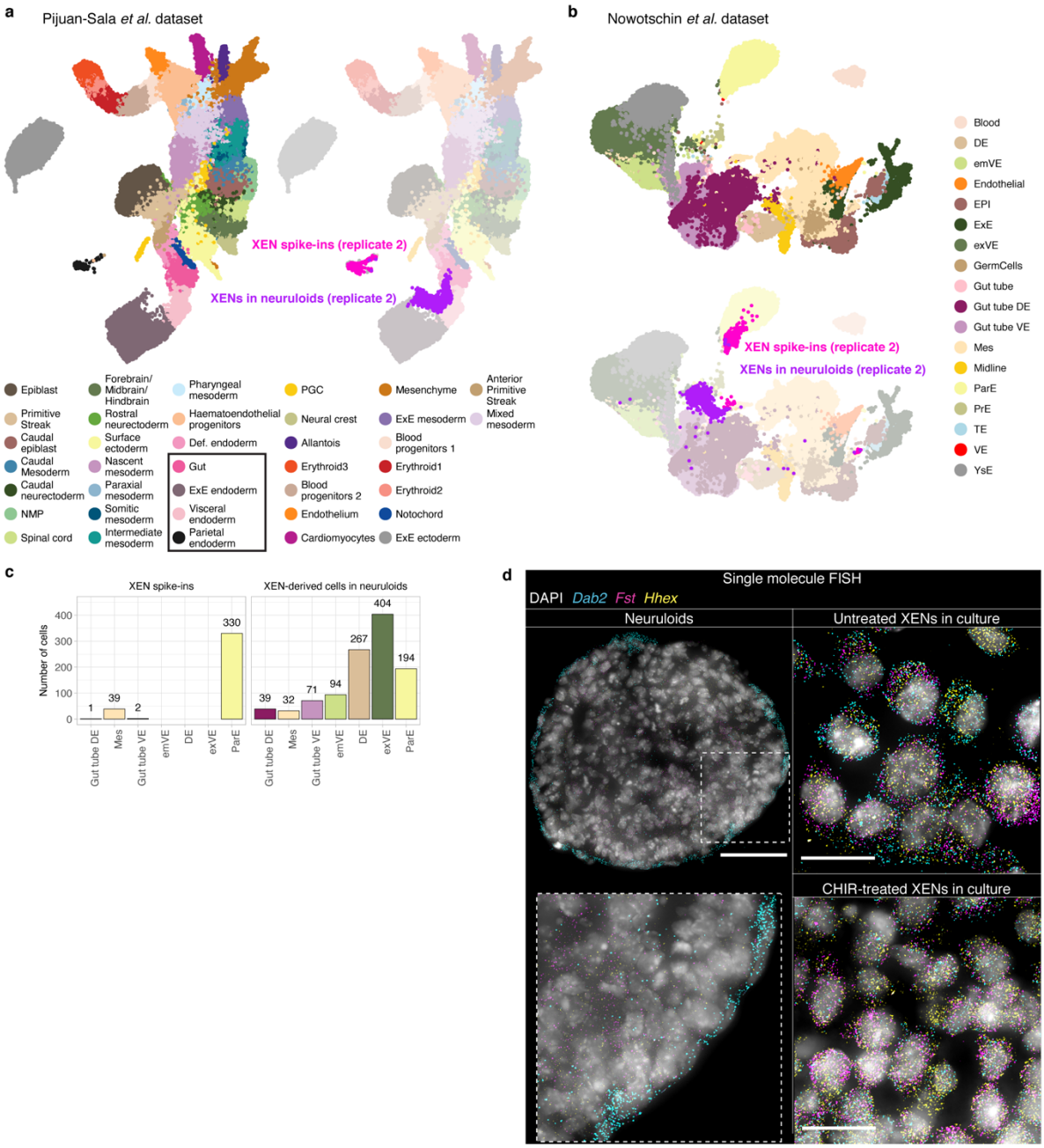

Extended data Fig. 6 | XEN-derived cells are visceral endoderm-like in neuruloids.

a, **b**, Umaps of the Pijuan-Sala or Nowotschin dataset, respectively. XEN spike-ins and XEN-derived cells from neuruloids replicate 2 (bright colors) are mapped to the *in vivo* datasets (dim colors). Framed cell types correspond to the ones on which the XEN cells mapped. **c**, Cell type frequencies of XEN spike-ins and XEN derived cells in neuruloids, resulting from knn assignments based on the mapping in **(b)**. **d,** *Dab2*, *Fst* and *Hhex* expression visualized by single molecule fluorescence *in situ* hybridization (smFISH). Cell nuclei were stained with DAPI. Each diffraction limited dot is a single mRNA molecule. Left, section of a neuruloid at 96 h. Scale bar 50 µm. Right, XEN cells cultured under standard maintenance conditions (top) and XEN cells treated with CHIR according to the neuruloid protocol (bottom). Scale bars 20 µm.

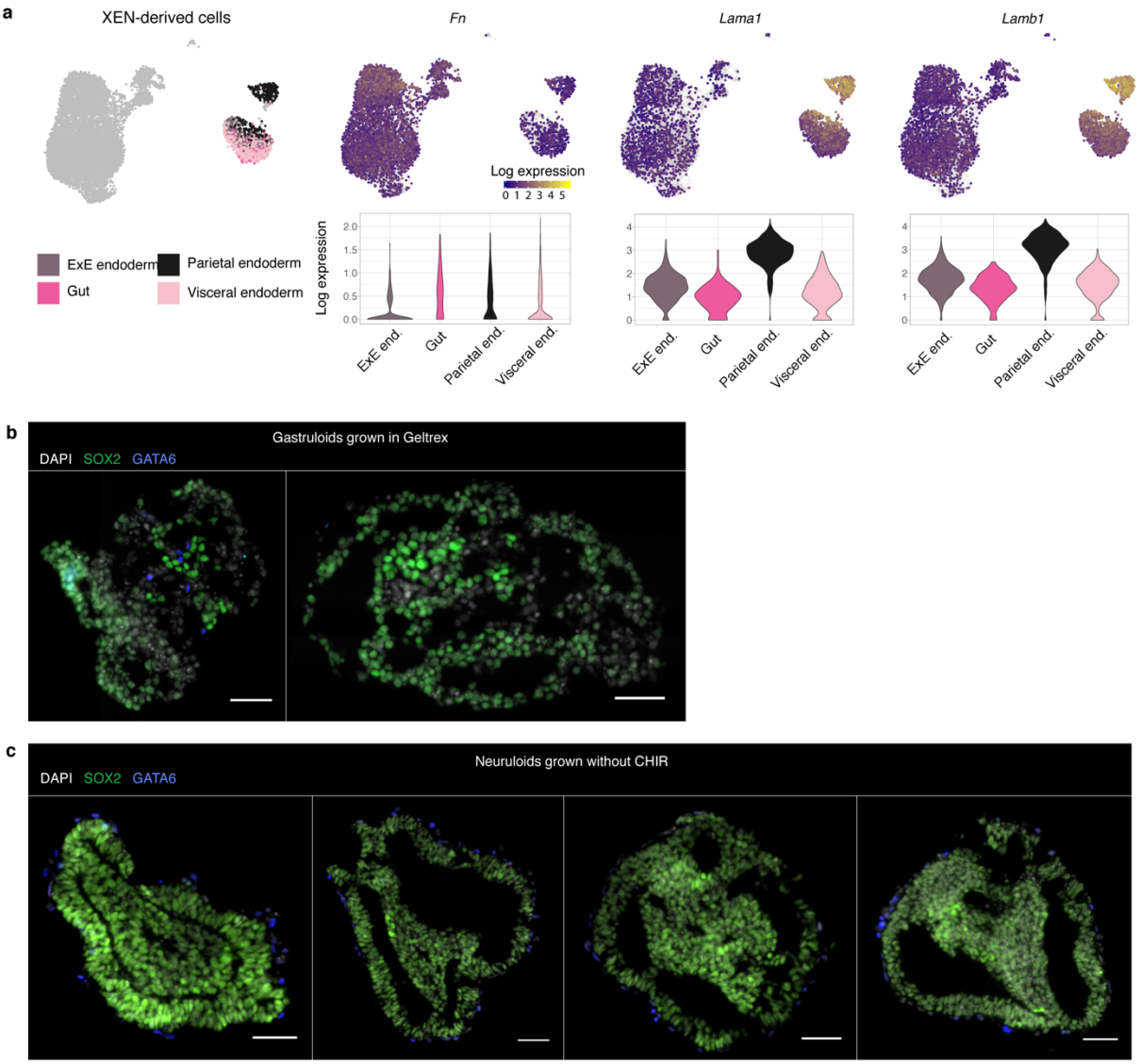

Extended data Fig. 7 | XEN cells induce stratified epithelium and lumen formation

a, Left, umap of cells in neuruloids with XEN-derived cells colored by cell type (gut, parietal endoderm (parietal end.), embryonic VE (visceral end.) or extraembryonic VE (ExE end.)). Mid-right, umap of cells in neuruloids colored by log expression of Fibronectin (*Fn*), Laminin alpha 1 (*Lama1*) and Laminin beta 1 (*Lamb1*). A violin plot of log expression in XEN-derived cell types is shown below the umap for each gene. **b**, SOX2 and GATA6 immunostaining in sections of gastruloids grown in Geltrex at 96 h. **c**, SOX2 immunostaining in sections of neuruloids grown without CHIR. No specific T staining could be detected (data not shown). XEN cells were localized by expression of GATA6. **b**, **c**, Cell nuclei were stained with DAPI. Scale bars 50 µm.

Extended Data Table 1 | Genes differentially expressed between spinal cord-like cells and the other cells types in neuruloids.

Gene	Log FC	p.adjust	Reference
Ccnd2	1.684190185	1.37E-210	Lacomme, M., et al., (2012). *Molecular and Cellular Biology*
Crabp2	2.27328271	0	Ruberte, E., et al., (1992). *Development*
Id3	1.789970808	5.65E-118	Wine-Lee, L., et al., (2004). *Development*
Fabp7 (BLBP)	2.339513279	2.65E-148	Feng, L., Hatten, M. E., & Heintz, N. (1994). *Neuron*
Rfx4	2.066843727	3.40E-130	Ashique, A. M., et al. (2009). *Science Signaling*
Hoxb9	1.561341789	4.07E-126	Graham, A., Maden, M., & Krumlauf, R. (1991). *Development*
Cdh2	1.486458795	1.15E-114	Radice, G. L., et al., (1997). *Developmental Biology*
Msx3	1.925035016	3.06E-116	Misra, K., Luo, H., Li, S., Matise, M., & Xiang, M. (2014). *Development*
Pax6	3.403368474	4.04E-280	Jeong, J., & McMahon, A. P. (2005). *Development*
Fabp5	1.316127675	1.97E-241	Shimamoto, C., et al. (2014). *Human Molecular Genetics*
Sfrp2	1.677002264	9.74E-140	Misra, K., & Matise, M. P. (2010). *Developmental Biology*
Hes3	2.132129411	2.12E-147	Lobe, C. G. (1997). *Mechanisms of Development*
Ptn	2.50622717	0	Magdaleno, S., et al. (2006). *PLoS Biology*
Fgf15	2.131102328	2.17E-151	McWhirter, J. R., et al., (1997). *Development*
Irx3	1.957663655	1.71E-146	Lebel, M., et al. (2003). *Molecular and Cellular Biology*
Zic1	2.371434543	1.56E-148	Nagai, T., et al., (1997). *Developmental Biology*
Fgfbp3	2.502793725	1.10E-253	Yu, K., McGlynn, S., & Matise, M. P. (2013). *Development*
Hes5	2.152139781	9.35E-119	Hatakeyama, J., et al., (2004). *Development*
Map1b	1.46443751	3.03E-174	Fawcett, J. W., et al., (1994). *Neuroscience*
Gas1	1.676359071	1.03E-135	Allen, B. L., Tenzen, T., & McMahon, A. P. (2007). *Genes & Development*
Sox11	1.610646468	6.85E-208	Tanaka, S., et al., (2004). *Molecular and Cellular Biology*
Sox2	1.54213575	1.78E-148	Hoffmann, S. A., et al., (2014). *Development*
Sox1	2.143957789	5.90E-172	Hoffmann, S. A., et al., (2014). *Development*

Extended Data Table 2 | Genes differentially expressed between spinal cord-like cells in neuruloids and gastruloids.

Gene	Log FC	Expression summary	BMP signalling response	Reference
Msx1	2.84	Dorsal neural tube + small ventral domain	BMP (Lee, K. J., & Jessell, T. M. (1999))	Misra, K., et al., (2014). Duval, N., et al. (2014).
Spink1	2.59			
Pax3	2.53	Dorsal neural tube	BMP (Lee, K. J., & Jessell, T. M. (1999))	Kriks, S., et al., (2005).
Zic1	1.81	Dorsal neural tube	BMP (Lee, K. J., & Jessell, T. M. (1999))	Nagai, T., et al., (1997). Aruga, J.,et al., (2002).
Msx3	1.75	Dorsal neural tube	BMP4 (Shimeld, S. et al., (1996))	Misra, K., et al., (2014). Duval, N., et al. (2014).
Crabp1	1.47	Forebrain, Neural crest + dorsal neural tube	-	Ruberte, E., et al., (1991).
Sp5	1.37	Midbrain and dorsal neural tube	-	Andoniadou, C. L., et al. (2011). Dunty, W. C., et al., (2014).
Epha5	1.29	Dorsal and ventral	BMP2 (Yamada, T., et al., (2016))	Abdul-Aziz, N. M., et al., (2009). Ono, K., et al. (2014).
Rspo3	1.28	Forebrain, dorsal neural tube	-	Nam, J.-S., et al., (2007).
En1	1.27	Hinbrain/Midbrain Ventral neural tube	Not affected by BMP (Timmer, J. R., et al., (2002))	Ericson, J., et al. (1997). Sgaier, S. K., et al., (2007).
Zic5	1.23	Dorsal neural tube and head fold	BMP (Nakata, K., et a., (2000))	Inoue, T., et al., (2004).
Fabp7 (BLBP)	1.14	Ventral neural tube Midbrain	-	Delile, J., et al., (2019). Feng, L., et al., (1994).
Id3	1.10	The roof plate and dorsal neural ectoderm + small ventral domain	BMP (Wine-Lee, L., et al., (2004))	Wine-Lee, L., et al., (2004).
Zic2	1.09	Dorsal neural tube	BMP6/7 (Lee, K. J., & Jessell, T. M. (1999))	Ybot-Gonzalez, P., et al., (2007). Sanchez-Ferras, O., et al., (2014).
Gadd45a	1.08	Mostly dorsal neural tube Residual expression in ventral neural tube	BMP2 (Ijiri, K., et al. (2005))	Kaufmann, L. T., et al., (2011).
Id1	1.04	Roof plate and dorsal neural ectoderm + small ventral domain	BMP (Wine-Lee, L., et al., (2004))	Wine-Lee, L., et al., (2004).
Cdh11	0.98	Neural crest + dorsal neural tube	BMP7 (Awazu, M., et al., (2017))	Tondeleir, D., et al., (2014). Kashef, J., et al., (2009).
Lhx1	0.97	Dorsal interneurons	Not affected by BMP4/7 (Le Dréau, G., et al., (2012))	Le Dréau, G., et al., (2012).
Fgf15	0.95	Dorsal regions of the di-, mes and metencephalon	-	McWhirter, J. R., et al., (1997). Fischer, T., et al., (2011).

Extended data Table 3 | Genes differentially expressed between XEN-derived cells in neuruloids and cultured XEN cells.

Gene	Log FC	Expression summary	Reference
Apoe	-1.80	VE > PE	Basheeruddin, K., et al., (1987)
H19	-1.69	VE > PE	Long, L., & Spear, B. T. (2004).
Spink1	-1.66	VE	Goh, H. N., et al. (2014).
Emb	-1.33	pan-endoderm	Brown, K., et al., (2010).
Cited1 (Mgs1)	-1.07	exVE	Dunwoodie, S. L., et al., (1998).
Rdx (Radixin)	-0.83	VE	Igarashi, H., et al. (2018). McClatchey, A. I., et al.,(1997).
Anxa4	-0.78	pan-endoderm	Brown, K., et al., (2010).
Dpp4	-0.68	VE	Sherwood, R. I., et al. (2007).
Lapr1 (Lpa1)	-0.57	VE	Koike, S., et al., (2009).
Rnf128 (Greul)	-0.56	VE	Borchers, A. G. M., et al., (2002).
Gata4	0.77	pan-endoderm	Morrisey, E. E., et al.,(1998).
P4ha2	0.79	PrE	Ohnishi, Y., et al. (2014).
Adamts9	1.08	PE	Jungers, K. A., et al., (2005).
Lamb1	1.51	PE	Miner, J. H., et al., (2004).
Sparc	1.51	PE	Mason, I. J., et al., (1986).
Lama1	1.54	PE	Hogan, B. L., et al., (1980).
Fabp3	1.60	exVE - PE	Cheng, S., et al. (2019). Futaki, S., et al. (2003).
Lamc1	1.89	PE	Smyth, N., et al., (1999).
Fst	1.99	PE	Feijen, A., et al. (1994).